1-1-2016

# Electrical stimulation enhances the acetylcholine receptors available for neuromuscular junction formation

Rodrigo Lozano
*University of Wollongong*, rl137@uowmail.edu.au

Kerry J. Gilmore
*University of Wollongong*, kerryg@uow.edu.au

Brianna C. Thompson
*University of Wollongong*, brianna@uow.edu.au

Elise M. Stewart
*University of Wollongong*, elises@uow.edu.au

Aaron Waters
*University of Wollongong*, amw844@uowmail.edu.au

*See next page for additional authors*

# Electrical stimulation enhances the acetylcholine receptors available for neuromuscular junction formation


## Abstract

Neuromuscular junctions (NMJ) are specialized synapses that link motor neurons with muscle fibers. These sites are fundamental to human muscle activity, controlling swallowing and breathing amongst many other vital functions. Study of this synapse formation is an essential area in neuroscience; the understanding of how neurons interact and control their targets during development and regeneration are fundamental questions. Existing data reveals that during initial stages of development neurons target and form synapses driven by biophysical and biochemical cues, and during later stages they require electrical activity to develop their functional interactions. The aim of this study was to investigate the effect of exogenous electrical stimulation (ES) electrodes directly in contact with cells, on the number and size of acetylcholine receptor (AChR) clusters available for NMJ formation. We used a novel in vitro model that utilizes a flexible electrical stimulation system and allows the systematic testing of several stimulation parameters simultaneously as well as the use of alternative electrode materials such as conductive polymers to deliver the stimulation. Functionality of NMJs under our co-culture conditions was demonstrated by monitoring changes in the responses of primary myoblasts to chemical stimulants that specifically target neuronal signaling. Our results suggest that biphasic electrical stimulation at 250 Hz, 100 ¿s pulse width and current density of 1 mA/cm2 for 8 h, applied via either gold-coated mylar or the conductive polymer PPy, significantly increased the number and size of AChRs clusters available for NMJ formation. This study supports the beneficial use of direct electrical stimulation as a strategic therapy for neuromuscular disorders.



## Disciplines

Engineering | Physical Sciences and Mathematics

## Publication Details

Lozano, R., Gilmore, K. J., Thompson, B. C., Stewart, E. M., Waters, A. M., Romero-Ortega, M. & Wallace, G. G. (2016). Electrical stimulation enhances the acetylcholine receptors available for neuromuscular junction formation. Acta Biomaterialia, 45 328-339.



## Authors

Rodrigo Lozano, Kerry J. Gilmore, Brianna C. Thompson, Elise M. Stewart, Aaron Waters, Mario I. Romero-Ortega, and Gordon G. Wallace

Elsevier Editorial System(tm) for Acta Biomaterialia

Manuscript Draft

Manuscript Number: AB-16-660R2

Title: Electrical stimulation enhances the acetylcholine receptors available for neuromuscular junction formation

Article Type: Full length article

Keywords: electrical stimulation; conductive polymer; acetylcholine receptors; neuromuscular junction

Corresponding Author: Prof. Gordon G Wallace, Ph.D.

Corresponding Author's Institution: University of Wollongong

First Author: Rodrigo Lozano

Order of Authors: Rodrigo Lozano; Kerry J Gilmore, PhD; Brianna C Thompson, PhD; Elise M Stewart, PhD; Aaron M Waters; Mario Romero-Ortega, PhD; Gordon G Wallace, Ph.D.

Abstract: Neuromuscular junctions (NMJ) are specialized synapses that link motor neurons with muscle fibers. These sites are fundamental to human muscle activity, controlling swallowing and breathing amongst many other vital functions. Study of this synapse formation is an essential area in neuroscience; the understanding of how neurons interact and control their targets during development and regeneration are fundamental questions. Existing data reveals that during initial stages of development neurons target and form synapses driven by biophysical and biochemical cues, and during later stages they require electrical activity to develop their functional interactions. The aim of this study was to investigate the effect of exogenous electrical stimulation (ES) electrodes directly in contact with cells, on the number and size of acetylcholine receptor (AChR) clusters available for NMJ formation. We used a novel in vitro model that utilizes a flexible electrical stimulation system and allows the systematic testing of several stimulation parameters simultaneously as well as the use of alternative electrode materials such as conductive polymers to deliver the stimulation. Functionality of NMJs under our co-culture conditions was demonstrated by monitoring changes in the responses of primary myoblasts to chemical stimulants that specifically target neuronal signaling. Our results suggest that biphasic electrical stimulation at 250 Hz, 100 µs pulse width and current density of 1 mA/cm2 for 8 h, applied via either gold-coated mylar or the conductive polymer PPy, significantly increased the number and size of AChRs clusters available for NMJ formation. This study supports the beneficial use of direct electrical stimulation as a strategic therapy for neuromuscular disorders.

# Electrical stimulation enhances the acetylcholine receptors available for neuromuscular junction formation.

Rodrigo Lozano[1], Kerry J. Gilmore[1], Brianna C. Thompson[1], Elise M. Stewart[1], Aaron M. Waters[1], Mario Romero-Ortega[2], Gordon G. Wallace[1*]

[1]Intelligent Polymer Research Institute, ARC Centre of Excellence for Electromaterials Science, AIIM Facility, University of Wollongong, Wollongong, NSW 2522, Australia.
[2]Department of Bioengineering, University of Texas at Dallas, Richardson, TX 75080, USA.
*Corresponding author.

## Abstract

Neuromuscular junctions (NMJ) are specialized synapses that link motor neurons with muscle fibers. These sites are fundamental to human muscle activity, controlling swallowing and breathing amongst many other vital functions. Study of this synapse formation is an essential area in neuroscience; the understanding of how neurons interact and control their targets during development and regeneration are fundamental questions. Existing data reveals that during initial stages of development neurons target and form synapses driven by biophysical and biochemical cues, and during later stages they require electrical activity to develop their functional interactions. The aim of this study was to investigate the effect of exogenous electrical stimulation (ES) electrodes directly in contact with cells, on the number and size of acetylcholine receptor (AChR) clusters available for NMJ formation. We used a novel *in vitro* model that utilizes a flexible electrical stimulation system and allows the systematic testing of several stimulation parameters simultaneously as well as the use of alternative electrode materials such as conductive polymers to deliver the stimulation. Functionality of NMJs under our co-culture conditions was demonstrated by monitoring changes in the responses of primary myoblasts to chemical stimulants that specifically target neuronal signaling. Our results suggest that biphasic electrical stimulation at 250 Hz, 100 µs pulse width and current density of 1 mA/cm$^2$ for 8 h, applied via either gold-coated mylar or the conductive polymer PPy, significantly increased the number and size of AChRs clusters available for NMJ formation. This study supports the beneficial use of direct electrical stimulation as a strategic therapy for neuromuscular disorders.

## Introduction

Contractile muscle activity is controlled by the motor neuron-muscle system [1]. The regulation of this system involves the transmission of action potentials from the central nervous system to peripheral nervous system then to muscle fibers via neuromuscular junctions (NMJs) [2, 3]. This complex system relies on dynamic interactions of signaling molecules and cell membrane proteins [4, 5] to release neurotransmitters from motor neurons into the synaptic cleft, followed by neurotransmitter binding to specific receptors (AChR) that are located within the plasma membrane of muscle fibers [6, 7]. There are many factors to be considered when investigating NMJ formation, maturation and function, however recent data reveals that clustering and maintenance of high densities of AChRs are key elements of synaptogenesis at the NMJ [8-11].

Recent reviews support the idea that dysfunction of these junctions may play a key role in several neuromuscular diseases, for example growing evidence supports the “dying-back” hypothesis of amyotrophic lateral sclerosis (ALS) suggesting that the survival of NMJs is essential to delay the progression of ALS [12]. It has also been suggested that stabilization of NMJs is a promising approach to attenuate the development of muscle wasting disorders, indicating that NMJs are good markers of motor neuron health [13]. Therefore, therapeutic

treatments aimed at maintaining NMJs may be an effective approach to slowdown the progression of these diseases.

Recent literature reviews suggest that during development neurons target and form synapses driven by dynamic interactions of biophysical and biochemical cues, whilst electrical activity, in the form of ion transients, plays a role in neuronal development both before and after synapse formation [4, 14, 15]. Many *in vitro* and *in vivo* studies have been conducted using external electrical stimulation (ES) to control cell characteristics [7, 16], indicating that ES has positive benefits in many areas such as wound-healing [16], bone growth [17], pain relief, muscle restoration [18, 19], proliferation and differentiation of stem cells [20], as well as in nerve guidance and growth [21, 22]. In addition, it has recently been shown that the formation and architecture of NMJs can be influenced by electrical stimulation (ES) *in vitro* [23] and *in vivo* [24, 25], however, most of these stimulations relied on direct current which has been shown to generate faradic reactions allowing charge leakage through the electrodes, and compromising the safety of cells and tissues [26]. Therefore establishment of a system that delivers efficient and safe electrical stimulation to cells and tissues is needed. The system should deliver optimized parameters such as stimulation time, current amplitude, stimulus mode and electrode material to achieve the desired outcomes for a range of excitable tissues.

An extensive series of materials has been used as electrodes to deliver electrical stimulation including stainless steel, titanium nitride, gold, platinum, platinum-iridium alloys and tungsten. These are materials that have been identified as safe, however according to previously published studies, electrical stimulation using some of these metallic materials can generate unwanted by-products commonly called "faradaic products" due to oxidation-reduction of components in the surrounding media [27]. Some metal electrodes are also prone to dissolution due to corrosion processes making it difficult to evaluate the true effect of the ES on cells [28].

Conducting polymers (CP) offer the possibility to improve the interaction of electrodes with biological systems by improving cell biocompatibility as well as avoiding the issues associated with electrolysis and corrosion [29, 30], while providing a sufficiently low impedance electrode for cell stimulation. Furthermore, these "smart materials" as they have been called [29] offer many more advantages over metal electrodes, due to their physical, chemical and electrical properties which can be custom designed to fit specific applications [29, 31, 32]. CPs as electrode coating materials facilitate enhanced integration of electrodes with cells and tissues [20, 33-36]. This is achieved by increased surface area, reduced impedance as a result of improved charge transfer and reduced inflammatory responses due to the modification of surface roughness [37]. In addition, CPs offer the capability to incorporate biological molecules, such as growth factors, enzymes, antibodies and DNA [38, 39] into the polymer and release them locally in a controlled manner [38, 40-42].

Since it was first described by Bolto in the 1960s [43], polypyrrole (PPy) is one of the CPs most extensively investigated for tissue engineering applications [43]. PPy is an amorphous and opaque material that has high electrical conductivity, ion exchange capacity, good environmental stability [34, 37, 39, 44-46], but most importantly, it can be synthesized and modified in many ways, making it attractive for a wide range of applications [19, 41]. One of the many remarkable benefits of this polymer is its electrical properties which can be attributed to the fast, facile ability to switch between different oxidation states [39]. PPy doped with dodecyl benzene sulphonate (DBS) has previously been shown by our group to enhance neuronal stem cell and muscle cell differentiation [19, 20] as well as facilitate the controlled release of growth factors as treatments for nerve injuries to prevent nerve degradation and promote nerve protection [40].

In this study we propose an innovative *in vitro* model to investigate effects of ES on NMJ formation by exposing primary myoblast /motor neuron co-cultures to electrical stimulation, utilizing the conductive polymer polypyrrole doped with DBS to deliver the stimulus. The polymer properties were characterized using atomic force microscopy (AFM), scanning electron microscopy (SEM) and impedance measurements. Immunohistochemistry and confocal microscopy were employed to determine the increase in number and size of AChR clusters, which was further supported by analysis of cell lysates for NMJ-associated proteins by Western blotting. We demonstrated the functionality of the NMJ model by monitoring the responses to neuronal stimulation using calcium imaging as well as observations of muscle twitching. This *in vitro* model provides a tool for further investigation of the delivery of either direct or field electrical stimulation to the cells, and allows many different stimulation strategies to be assessed simultaneously. This model was used to establish a positive effect of ES using the conductive polymer PPy/DBS at 250 Hz /1 $mA/cm^2$ current density for 8 h using biphasic 100 µs pulses on NMJ formation, increasing the number and size of AChR clusters, as well as increasing the expression of the NMJ-associated proteins Rapsyn and Synapsin.

## Material and methods

### Preparation of polymer films

Pyrrole (Py) monomer was obtained from Sigma-Aldrich and distilled before use. The dopant dodecyl benzene sulfonate (DBS) was obtained from Sigma-Aldrich. Gold coated mylar (Solutia Performance Films) was prepared for polymerization by cleaning with isopropanol and rinsing with distilled water. Distilled Py (0.2 M) was mixed with DBS solution (0.05 M) in Milli-Q water, and PPy films were polymerized galvanostatically from this solution using a standard three-electrode electrochemical cell. Gold coated mylar films were used as the working electrode (WE), a platinum mesh as a counter electrode (CE), and a Ag|AgCl reference electrode (RE) were connected to an eDAQ EA161 potentiostat. The polymer was galvanostatically grown at 0.1 $mA/cm^2$ current density for 10 min according to a previous report from our group [20]. After polymerization, the films were rinsed with Milli-Q water and allowed to dry before use.

### Atomic force microscopy

AFM images were taken using JPK NanoWizard II BioAFM (JPK, Germany) with samples submerged in phosphate buffered saline (PBS) solution. Images were taken using a silicon nitride cantilever with a spring constant of 0.42 $Nm^{-1}$ in AC mode. Scans of 10 and 1 µm square areas were taken at 0.5–1 Hz rate and sampling sizes of 512 x 512 pixels. The root mean square (RMS) roughness ($R_q$) and the average roughness ($R_{ave}$) values were obtained using JPK image processing software.

### Impedance measurements

The impedance of gold coated mylar and PPy/DBS gold coated mylar electrodes were measured and calculated using electrochemical impedance spectroscopy (EIS). The experiments were performed in PBS (pH 7.2) at room temperature using a three electrode cell comprising gold coated mylar or PPy/DBS gold coated mylar as working electrode, platinum mesh as counter electrode and a Ag/AgCl (3.0 M NaCl) reference electrode. Three independent measurements (n=3) were performed on each material using a CHI EIS system (Model 600 D, CH instruments, Inc) connected to CHI software version 16.02. The impedance spectra were obtained over the frequency range 0.01 Hz to 100 kHz with AC amplitudes of ± 10 mV and ± 50 mV versus the reference electrode. This value was chosen as it has been reported to avoid the redox activity region of the polymer [19, 21].

Materials and electrodes used for the impedance experiments were treated in the same way as for the ES experiments involving cells. COMSOL Multiphysics (version 5.0, Electric Currents Interface) was used to simulate the current flow within the cell stimulation module in order to assess the uniformity of current flow across the working electrode (assumed to be perfectly conducting) for this particular module design.

**Surface preparation for cell culture**.

The electrical stimulation (ES) was performed using a parallel two electrode setup as shown in Fig. 4. The gold coated mylar (or PPy) formed the working electrode and a platinum mesh electrode was used as the auxilary electrode. The ES devices were rinsed and soaked with 70% ethanol for 30 min in a sterile environment. The ethanol was removed; samples were allowed to dry, followed by two washes and an overnight soak in DMEM to remove any chemical residues. The media was removed and the wells were coated overnight with 2 µg/mL laminin (Life Technologies) in DMEM at 4 °C. Excess laminin was removed and wells allowed to dry prior to cell seeding.

**Electrical stimulation equipment**

Electrical stimulation was performed using a Digital DS8000 Stimulator equipped with A365 Isolator units (World Precision Instruments), interfaced with an e-corder system (eDAQ) and the parallel two-electrode setup shown in Fig. 4. The two electrodes consisted of a working electrode (PPy/DBS or gold coated mylar -1 x 1.8 cm) and auxiliary electrode (platinum mesh). The cells were stimulated using a starting stimulation paradigm previously found to be beneficial for neuronal differentiation and guidance [35, 41], consisting of current pulses of 1 $mA/cm^2$ with a biphasic waveform, consisting of 100 µs pulses with 20 µs interphase open circuit and 3.78 ms short circuit phase, at a frequency of 250 Hz (Fig. 4B). A range of frequencies including 250 Hz, 20 Hz and 0.5 Hz were tested and the optimal frequency was obtained. We then kept the frequency constant at the optimal frequency and tested a range of current amplitudes: 1 $mA/cm^2$, 0.1 $mA/cm^2$ and 0.01 $mA/cm^2$. We obtained the optimal amplitude, and then tested a range of durations of stimulation such as 8 h, 4 h, and 2 h under the optimal frequency and current regimes. Each parameter was tested in three independent experiments. For these experiments treated cells were compared to designated control samples which consisted of non-electrically stimulated (NES) cells (seeded on gold coated mylar or PPy/DBS). The optimized electrical stimulation regimen (frequency, amplitude and duration) was subsequently used to test the difference between electrode materials (PPy/DBS vs. uncoated gold-mylar). For these experiments controls were NES on PPy/DBS and NES on gold coated mylar. After ES applications, cells were fixed for immunostaining or prepared for other analyses.

**Cell culture**

The co-culture is a homologous (both cells are from same species) model that included a primary myoblast cell line (kindly donated by Prof. Robert Kapsa, St Vincent's Hospital, Melbourne, Australia) [19] in conjunction with the well-characterized motor neuron NSC-34 cell line [47], which is a fusion of neuroblastoma with mouse primary motor neuron cells [48] (kindly provided by Dr. Justin Yerbury, University of Wollongong, Australia). Primary myoblast cultures were generated from the hindlimb skeletal muscle of C57BL10J-SVHM$^{\beta Gal}$ mice (BL10J$^{\beta Gal}$ mice), derived from GTROSA26 (C57BL6) backcrossed (11$^{th}$ generation currently) onto a C57BL10J mouse genetic background. These mice bear a LacZ reporter transgene cassette and were used in these experiments to accommodate *in vivo* tracking of donor cells in future implantation experiments for NMJ-promoting regenerative constructs [19]. Primary myoblast cells were maintained in a proliferation medium containing Ham's F-10 medium, supplemented with 2.5 ng/mL bFGF (Peprotech) and 20% fetal bovine serum (FBS, Invitrogen supplied by Life Technologies), and 1% penicillin/ streptomycin (P/S, Life

Technologies). On the other hand, the NSC-34 cells were maintained using 1:1 Dulbecco's modified Eagle's medium (DMEM) and F-12 media, supplemented with 10% fetal bovine serum (FBS), and 1% P/S.

Prior to co-culture, both primary myoblast and NSC-34 cells were exposed to two different cell differentiation culture media in addition to the standard media for each cell type in order to determine the most appropriate media for co-culture maintenance. Primary myoblast cells were exposed to NSC-34 cell differentiation media (1:1 DMEM and F-12 media, supplemented with 3% fetal bovine serum (FBS), and 1% P/S) as well as to media containing a 1:1 mixture of primary myoblast (DMEM supplemented with 2% horse serum (HS), and 1% P/S) and NSC-34 cell differentiation media. The same approach was used with NSC-34 cells, which were grown using primary myoblast cell differentiation media and 1:1 mixture of primary myoblast and NSC-34 cell differentiation media (data not shown). No major morphological changes were observed on primary myoblast differentiation when they were exposed to the NSC-34 differentiation media or to the 1:1 mixture of the NSC-34/primary myoblast differentiation media. On the other hand, small amount of clustering of differentiated NSC-34 cells was observed when exposed to the primary myoblast differentiation media and to the mix 1:1 NSC-34/primary myoblast differentiation media. Due to these findings, NSC-34 differentiation media was used for the co-cultures. For electrical stimulation experiments on the co-cultures, primary myoblast cells were seeded at 30,000 cells/cm$^2$ and allowed to differentiate for 3 days using medium consisting of 1:1 DMEM and F-12, supplemented with 3% FBS, and 1% P/S (NSC-34 differentiation media). After 3 days NSC-34 cells were added to the differentiated muscle cultures at 5,000 cells/cm$^2$ and maintained in the differentiation media (1:1 DMEM and F-12 media, supplemented with 3% fetal bovine serum (FBS) and 1% P/S) for 4 days at 37 °C in 5% $CO_2$. At the end of the 4 days co-cultures (7 day total) were electrically stimulated using parameters state above For mono-cultures (primary myoblast and NSC-34) cells were seeded at 30,000 and 5,000 cells/cm$^2$ respectively, also maintained and electrically stimulated as for co-cultures.

**Scanning electron microscopy (SEM)**

Control cells were fixed at room temperature using 3.7% paraformaldehyde (PFA) solution in PBS for 10 min followed by dehydration using an ethanol series. After dehydration, samples were exposed to a critical point drying process using a Leica EM CPD030 instrument, and then gold coated using an Edwards sputter coater (15 nm layer). Samples were kept in a desiccation cabinet until images were obtained. For images of PPy/DBS or gold coated mylar films (without cells), samples were exposed to a dehydration and critical point drying process as above. SEM studies of the samples were carried out using the JSM-7500 Scanning Electron Microscope installed at the Electron Microscopy Centre (EMC, University of Wollongong).

**Neuromuscular junction functional analysis**

To confirm the functionality of mono-cultures (muscle and nerve) and co-cultures, calcium transients in cells were visualized using confocal microscopy before and after chemical stimulation (neuronal activation) [49, 50]. Cells were incubated for 20 min at 37 °C in a 2 µM solution of Fluo 4-AM (Life Technologies), then cells were rinsed and mounted onto a Leica TSC SP5 II confocal microscope, under controlled temperature and $CO_2$ conditions. Cells were immediately transferred into an artificial extracellular solution reported in [51] and consisting of 137 mM NaCl, 1.3 mM $CaCl_2$, 5.4 mM KCl, 0.44 mM $KH_2PO_4$, 0.5 mM $MgCl_2$, 0.4 mM $MgSO_4$, 0.3 mM $NaHPO_4$, 4 mM $NaHCO_3$, 5.6 mM D-glucose, 10 mM HEPES and 0.02 mM EDTA at 7.4 pH prior to chemical stimulation. Primary myoblast cells were stimulated using high (70 mM) potassium by increasing the KCl concentration from 5.4 to 75.4 mM and decreasing the NaCl concentration from 137 mM to 67 mM to maintain ionic strength. In addition both NSC-34 cells and the co-cultures were chemically stimulated with a

final concentration of 1.5 mM glutamic acid (Sigma) [52]. As cells were loaded with Fluo-4 AM, each response to chemical stimulation (glutamic acid or potassium) generated a change in green fluorescence which was analyzed using time-lapse images, at specified individual regions of interest (ROI) that are large enough to cover the cell. This was achieved using the regions of interest (ROIs) tool of LAS AF version 2.6.0 software (Leica) and was analyzed in three independent experiments.

**Fixation and Immunocytochemistry**

Prior to immunostaining, the NSC-34 cells were fixed with 3.7% PFA for 10 min, followed by permeabilization and blocking with 0.3% Triton-X-100 in PBS with 10% donkey serum for 1 h at room temperature. Cells were washed for 5 mins, three times in 0.1% Tween 20 in PBS. This was followed by primary antibody incubation in 10% donkey serum in PBS. Primary antibodies were mouse anti-neurofilament (1:1000, Millipore) and sheep anti-HB9 (1:200, Abcam). After an overnight incubation of the primary antibody at 4 °C, 3 washes with 0.1% Tween 20 in PBS (5 min each) were performed, then secondary antibodies (Alexa Fluor 488 conjugated donkey anti-sheep ThermoFisher Scientific), Alexa Fluor 555-conjugated donkey anti-mouse (ThermoFisher Scientific)) were added at 1:1000 dilution in PBS with 10% donkey serum. After 1 h incubation, 1 µg/mL DAPI in PBS (Molecular probes) staining was performed for 10 min. Finally, the cells were washed three times in PBS and mounted on cover slips using ProLong Gold Antifade Reagent (ThermoFisher Scientific) for imaging using a Leica TSC SP5 II confocal microscope.

For co-cultures, cells were fixed, permeabilized, blocked and washed using methods described above. Primary antibodies were mouse anti-desmin (1:100, Novocastra) and chicken anti-beta-III-tubulin (1:1000, Millipore). After an overnight incubation of the primary antibody at 4 °C, 3 washes with PBS (5 min each) were performed, then secondary antibodies at 1:1000 dilution (Alexa Fluor 488 conjugated donkey anti-chicken (ThermoFisher Scientific), Alexa Fluor 594-conjugated goat anti-mouse (ThermoFisher Scientific), Alexa Fluor 555-conjugated goat anti-rabbit) and alpha–bungarotoxin Alexa Fluor 647 conjugate (1:500, Life Technologies) were added in PBS with 10% donkey serum. DAPI incubation and final preparation was performed as stated above.

**Quantification of acetylcholine receptor (AChR) clusters**

For the quantification and analysis of the AChR clusters, we used computer software to identify the receptors applying similar methodology as previously described [11, 53]. This method comprises three main steps: 1) imaging using confocal microscopy, 2) conversion of images to 16 bit grayscale, 3) image analysis using MetaMorph software V 7.8. (Coherent Scientific). Briefly, we took 20 random images from each well for 3 independent experiments (n=3). In accord with a previous report [11], the threshold size for AChR clusters was 5 $\mu m^2$ in area. The total number of AChR clusters and the sizes of clusters were counted and measured. The results were expressed as the total number of AChR cluster per $mm^2$ and the cluster areas in $\mu m^2$.

**Western blot analysis**

We monitored the increase in the protein-level expression of Rapsyn and Synapsin on the post-synaptic (primary myoblast) as well as the pre-synaptic (nerve-associated) side of the NMJ respectively. The effect of electrical stimulation on the expression levels of both of these proteins was assessed by cell lysis and protein isolation in NET buffer (20 mM Tris, 100 mM NaCl, 1 mM EDTA, 0.5% Triton X-100 ), with subsequent protein quantitation using the Pierce BCA assay (Sigma-Aldrich). 20 µg total protein was loaded onto a Mini-protean pre-cast 12% gel (Bio-Rad) and subjected to SDS-PAGE, followed by semi-dry transfer to nitrocellulose membranes. After blocking in 5% BSA (Sigma) in tris-buffered saline/0.05%

Tween-20 (TBST), blots were probed with rabbit anti-Rapsyn (1:500) or anti-Synapsin (1:500) antibodies (Abcam) overnight at $4^0$C in 3% BSA/TBST, washed in TBST containing 0.1% Tween-20, then incubated for 1 h at room temperature in HRP-conjugated anti-rabbit (1: 3000) secondary antibodies in 3% BSA/TBST. The loading control beta-actin (1:5000) was used to normalize protein loading between wells, after assessing the linear range for ECL detection of each protein. ECL detection using Bio-Rad Clarity ECL reagent and the Bio-Rad Chemidoc system was followed by analysis of band intensities using ImageLab software (Bio-Rad). The expression levels of the target proteins Rapsyn and Synapsin were compared in 3 independent experiments for muscle mono-cultures and co-cultures and for 2 independent experiments in the case of nerve mono-cultures.

**Statistical analysis**

The measurement of AChR clusters was performed on three independent experiments. For co-cultures, 20 images were taken from each of 2 internal replicate wells in three independent experiments with a total of 60 images and 40 images for the mono-culture were taken. The statistical analysis for each parameter tested (frequency, amplitude, time and material) was assessed using one-way analysis of variance (ANOVA, IBM SPSS Statistics, version 21). Whenever homogeneity of variance (Levene's test > 0.05) was validated, Bonferroni post-hoc tests were used to assess the significance level of differences in numbers of AChR clusters. Where Levene's test was not satisfied, additional post-hoc tests including Welch and Brown-Forsythe tests were used to confirm that heterogeneity of variances did not affect the statistical significance of observed differences in these large datasets.

## Results and discussion

### Materials characterization

Evaluation and characterization of biomaterials is an essential aspect of understanding cell behavior since the quality of cell attachment to materials will determine the capacity of cells to proliferate and to differentiate [54]. We characterized the surface topography of the films at the micro- and nanoscales using SEM and AFM respectively (Fig. 1). At the microscale SEM images showed that films were smooth and continuous. At the nanoscale AFM images showed typical nodular features of PPy with an average roughness ($R_{ave}$) of 3.12 nm and an RMS ($R_q$) value of 4.26 nm, consistent with values previously reported [20], compared to $R_{ave}$ of 0.889 nm and $R_q$ 1.17 nm for gold coated mylar samples. The results indicated that PPy /DBS is approximately 3.5 times rougher than gold coated mylar, however it is still considered a relatively smooth polymer that has previously been shown to support high levels of primary myoblast adhesion and differentiation (even in the absence of cell adhesion molecules), making it a suitable substrate for muscle myogenesis [19]. The impedances of the gold coated mylar and polymer-coated films were calculated and compared in 3 independent experiments (Fig. 1G). Polymerization of Py/DBS reduced significantly the impedance of gold coated mylar, at the lowest frequency tested. A smaller change was observed at the higher frequencies, and this agrees with previous findings [19]. However, at our stimulation frequency (250 Hz) a relatively small reduction from 134 Ω to 69 Ω was observed.

Overall, these results suggested that coating the gold mylar with a thin PPy/DBS film increased the roughness of the electrodes and decreased the impedance. Previous studies have shown that an increase in surface roughness has a positive effect on cell adhesion and growth [19, 44], while decreasing the impedance enhances charge transfer from electrode to tissue [19]. Therefore the increased roughness and decreased impedance afforded by the PPy/DBS coatings can be utilized to advantage to improve tissue compliance and efficiency in an electrical stimulation scenario.

**Assessment of co-cultures**

Co-culture of dissociated motor neurons and muscle cells is a well-accepted *in vitro* model for the study of neuromuscular junctions (NMJs) [55-57]. This approach has revealed important interactions between motor neurons and muscle cells. To this end, we developed a homologous model using primary myoblast cells in conjunction with the motor neuron (NSC-34) cell line (Fig. 2). The co-culture formation was demonstrated by immunostaining (Fig.2 A, B) as well as SEM imaging (Fig. 2 C). The muscle cells differentiated to cover the entire electrode surface (1.8 $cm^2$) with myotubes after 3 days, providing a confluent layer for the support of NSC-34 cells in co-cultures. The motor neurons were added and allowed to differentiate on top of the differentiated muscle cells for 4 days (total 7 days). The motor neurons were capable of developing long processes on top of the muscle cells. The expected long processes of NSC-34 cells (positive to motor neuron specific marker HB9 (supplementary Fig. S1)) are shown in more detail in individual channels of the immunostaining (Fig. 2A) by βIII-tubulin staining (green). Also the differentiated muscles (fully covering the electrode area) are shown by desmin staining (red), alongside the identification of the AChRs clusters with alpha-bungarotoxin staining (purple). These results demonstrated the successful development of the co-cultures using NSC-34 cells and primary myoblasts.

**Functionality of NMJ**

It has been reported that muscle cells do not respond to glutamic acid stimulation, however when co-cultured with nerve cells a nerve-activated muscle response is observed, indicating functional NMJ formation [58]. Here we show that when differentiated NSC-34 cells were loaded with the Fluo 4-AM label, $Ca^{2+}$ fluctuations were recorded in response to neuronal stimulation (glutamic acid) as previously reported [49, 50]. Fig. 3A indicates two regions of interest (ROI) where fluorescence intensity was increased as $Ca^{2+}$ was released after stimulation by glutamic acid (video supplementary S2). Using the same technique we validated that differentiated muscle cells (myoblasts) alone do not respond to glutamic acid, as observed in Fig. 3B (supplementary video S3). Also, the fluctuation of an active muscle (twitching) did not change with addition of glutamic acid (red arrows). In contrast inactive muscle cells responded to the stimulation of high concentrations of potassium (70 mM, blue arrow) by showing fluctuations of $Ca^{2+}$ (orange ROI in Fig. 3B). Additionally, in accordance with reported data [11, 59] we observed frequent muscle contractions in the co-culture systems in the absence of any stimulus. To determine if neuromuscular interactions were present in the co-cultures , we stimulated motor neurons (NSC-34) by adding glutamic acid (1.5 mM), as observed in Fig 3C (video supplementary S4). After approximately 10-15 sec of stimulation the muscle activity stopped and was reinstated after a further 70 sec (approximately), believed to be caused by dissipation of the glutamic acid in the flow cell. The experiments with the glutamic acid were repeated 4 times in independent co-cultures with the same result. This response suggest the presence of neuromuscular interaction in our co-culture set ups, rather than a direct effect of glutamic acid on muscle twitching, since glutamic acid does not affect muscle fibers as previously reported [58].

**Electrical Stimulation**

Studies have shown that cellular behavior can be regulated by electrical stimulation [6, 8, 16, 60-62]. The configuration and protocol for cell culture and stimulation of co-cultures on gold mylar and on PPy/DBS is illustrated in Fig. 4. In this study we used an electrical stimulation set up (Fig. 4A), using a waveform consisting of biphasic pulses of 100 µs pulse width with 20 µs interphase open circuit and 3.78 ms short circuit phase, at a frequency of 250 Hz (Fig. 4B). A schematic representation of the set up for culturing and stimulating co-cultures and individual muscle and motor neuron cultures on DBS-doped PPy is illustrated in Fig. 4C.

Furthermore, we predicted that this novel set up would provide a more direct and evenly distributed stimulus across the entire cell population, compared to commonly reported inserted electrodes. This was demonstrated by COMSOL modelling (compare Fig. 4D with supplementary Fig. S2) which shows a more uniform current density for this set up. Note that the modeling assumes perfectly conducting electrodes and does not consider the effect of the cells themselves, which may affect the current distribution in practice.

**Effect of ES parameters on NMJ formation**

The effect of ES parameters, including frequency, pulse amplitude, duration and electrode material on the formation and size of AChR clusters were tested, maintaining 100 µs biphasic pulses separated by a 20 µs delay. Initially, the optimization of ES parameters was performed using the platform detailed in Fig 4 C with gold coated mylar as the working electrode. We first probed the effect of frequency including 250 Hz, 20 Hz and 0.5 Hz with a current density of 1 mA/cm$^2$ for 8 h. There was a statistically significant increase in the number AChR clusters using 250 Hz, ie. increased by 45%, 32% and 38% compared to the unstimulated control (NES), 20 Hz and 0.5 Hz respectively (Fig. 5A). One way ANOVA ($F$ (3, 235) = 30.5) and Bonferroni *post hoc* test determined that the groups differed significantly ($p< 0.01$). Although, the ES at 20 and 0.5 Hz increased the number of AChR clusters compared to the unstimulated control by 10 and 6% respectively; the increase was not statistically significant. Next, we kept the frequency constant at 250 Hz and tested three different current densities: 1, 0.1 and 0.01 mA/cm$^2$. We observed that the combination of 250 Hz and 1 mA/cm$^2$ provided an increase in AChR clusters of 22%, 25% and 43% compared to the unstimulated control group (NES), 0.1 mA/cm$^2$ and 0.01 mA/cm$^2$ respectively (Bonferroni post hoc confirmed by Welch's $F$ (3, 131.5) = 30.1 and Brown-Forsythe F(3, 214.9)= 34.6 with *post hoc* Games-Howell, both showing significant difference ($p< 0.01$) (Fig 5B). Furthermore, it was observed that when we compared the control (NES) to 0.1 mA/cm$^2$ a non-statistical reduction of 3% occurred, however when compared to 0.01 mA/cm$^2$ a statistically significant reduction of 14 % occurred. Next, we tested the duration of the ES including 8, 4 and 2 h of stimulation using the optimized frequency and current density of 250 Hz and 1 mA/cm$^2$. We found ES at 250 Hz with 1 mA/cm$^2$ for 8 h resulted in a significant increase (Bonferroni post-hoc confirmed by Welch's $F$ (3, 90.53) = 79.15 and Brown-Forsythe F(3, 181.03)= 105.42 both with Games-Howell *post hoc* $p< 0.01$) in the number of AChR clusters, as indicated by the 43% increase over the control group (NES). Also, 8 h of stimulation resulted in a statistically significant increase when compared to 4 h and 2 h of stimulation duration. Furthermore, it was observed that ES at 250 Hz at 1 mA/cm$^2$ using 4 h and 2 h had no significant effect when compared to controls (NES) (Fig. 5C), suggesting that there may be a threshold for the duration of stimulation to make a detectable change to the AChR clustering.

Subsequently, utilizing the optimized stimulation parameters we compared the effect that different electrode materials have in delivering ES. In this case we compared PPy/DBS with gold coated mylar. As expected from our previous results, a significant increase in AChR cluster numbers with ES on PPy/DBS compared to the unstimulated control (NES) on PPy/DBS was observed (Bonferroni confirmed with Games-Howell *post hoc* $p< 0.01$), however, when compared to ES applied through gold coated mylar the difference was not statistically significant in co-cultures (Fig. 6A) indicating that ES enhanced the number of AChR clusters independently of the electrode material. Furthermore, a significant increase in the number of AChR clusters was observed when ES was performed on muscle mono-cultures (Fig 6B), again independent of the electrode material. This suggested that the enhancement of AchR by electrical stimulation was independent of the presence of neuronal cells.

The expression and localization of a number of NMJ-associated proteins have been linked to the maturation of the NMJ. Western blotting has been previously reported as a semi-

quantitative technique for monitoring increases in the protein-level expression of Rapsyn, on the post-synaptic (myoblast) side of the NMJ, which is involved in post-synaptic differentiation including the clustering of AChR [5, 63] and as such is an indicator of increasing maturity of the NMJ. Increases in expression of the pre-synaptic (nerve-associated) protein Synapsin, have also been associated with maturation of the NMJ [64]. We investigated the effect of electrical stimulation on the expression of these proteins on PPy/DBS in co-culture and also in nerve and muscle monocultures. Fig. 6 shows an increase in expression of Rapsyn, in response to electrical stimulation of both co-cultures and muscle monocultures when normalized to the expression of the loading control β-actin. On average the expression of Rapsyn was enhanced 2 fold by electrical stimulation of co-cultures, and 1.25 fold in pure muscle cultures, relative to that in unstimulated parallel cultures (average from 3 independent experiments, Figure 6 C). The expression of Synapsin in pre-synaptic nerve also increased in response to electrical stimulation (average 3.5 fold increase in expression in two independent experiments); however this was only observed in pure nerve cultures. This can be explained by the low abundance of Synapsin which renders detection of this protein in cell lysates from co-cultures problematic.

**Effect of electrical stimulation on AchR cluster sizes**

NMJ functionality is highly correlated with its structure; therefore observations of morphology are essential for the understanding of NMJ physiology. AChR are known to cluster during the development of mature NMJs. Here we show, based on previous reports [3, 65, 66] what appears to be the ACh receptors in our co-cultures and primary myoblast mono-cultures controls using SEM. The receptors showed a typical oval plaque as previously reported indicating proper morphology (Fig. 7A, B). Furthermore, it has been shown that the formation of receptor (AChR) clusters on muscle cells can be induced by applying DC electric field [67]. Here, we investigated the effect of ES on the AChR cluster sizes in co-cultures (Fig. 7 C-D) as well as in muscle mono-cultures (Fig. 7 E-F) using confocal microscopy, followed by image processing using MetaMorph software, to measure the cluster sizes. Our results indicate that electrical stimulation, using our optimized parameters, affects the Ach cluster sizes in co-cultures by increasing the average area of each cluster by up to 47% (Student's t-test, $p \leq 0.05$) when compared to unstimulated controls. Similar effects were observed in the muscle mono-cultures (average area increase of 59%, Student's t-test, $p \leq 0.05$) indicating the positive effect of ES on AChR cluster sizes.

**Conclusion**

AChR clusters were significantly increased, both in number and in size, by ES in our co-culture model. It has been reported that postsynaptic AChR formation at the NMJ synapse is regulated by innervation, muscle electrical activity and proteins including agrin and laminin [11]. In addition it has been reported that different frequencies used for ES can influence different motor units. For example motor units of type I (tonic) have a lower firing frequency response than those of type II (phasic). Furthermore, they reported that stimulating muscles using frequencies below 30 Hz activated type I motor units, on the other hand, whenever stimulating muscle using frequencies greater than 100 Hz, type II motor units were activated [68, 69]. Here, we have demonstrated that ES using 250 Hz biphasic 100 µs pulses, at a current density 1 mA/cm$^2$ for 8 h increased the number of AChR clusters available for NMJ formation. In addition, using immunostaining we have shown that an external stimulus such as ES can significantly enhance the AChR cluster sizes. Furthermore the enhancement was retained when the stimulus was delivered through the conducting polymer, PPy/DBS, coated onto the gold mylar substrate.

While this study showed no further enhancement with the use of PPy, taking into account the known versatility of the conducting polymer and our finding that it performed as well as gold demonstrate that further development of PPy as an alternative to traditional metal electrodes in this application is warranted. The PPy/DBS platform provides control over redox reactions at the electrode surface, due to polymer oxidation and reduction avoiding the generation of unwanted electrochemical reaction products. Additionally, the organic nature of this platform makes it an ideal surface to attach biomolecules such as agrin, laminin and/or encapsulate appropriate growth factors to enhance the therapeutic effect.

It has been reported that expression of the postsynaptic protein Rapsyn, an AChR-associated protein, is essential for forming AChR clusters. We showed that ES using optimized parameters can enhance Rapsyn protein expression level. Our data also demonstrated that the presynaptic protein Synapsin, which promotes maturation of the NMJ, increased in expression in nerve mono-cultures under the influence of our optimal ES parameters, suggesting that ES may be utilized to enhance the maturation of the NMJ.

In conclusion, our results indicate that electrical stimulation using the appropriate parameters has the capability to increase the numbers and size of AChR clusters and therefore to enhance the development of NMJs. The conductive polymer PPy is a promising alternative to traditional metal electrodes in terms of avoiding electrolysis and corrosion. This electroactive material is readily modified to attach important biomolecules such as laminin [70, 71]) and opens up opportunities for the release of growth factors such as NT3 and BDNF to the exact site of stimulation. It has been reported previously that release of these factors from conducting polymers via electrical stimulation provides an additional avenue to enhance the behavior of cultured cells [38, 40-42]. This opens up a new set of opportunities to combine ES with control bioactivity to further enhance NMJ formation and is the subject of ongoing work in our laboratories.

***Acknowledgements***

The authors would like to thank the Australian Research Council Centre of Excellence Scheme (CE140100012) for their funding of this research. In addition, we are also grateful to the ARC for support under the Australian Laureate Fellowship scheme (FL110100196) and the Consejo Nacional de Ciencia y Tecnologia (CONACYT, Mexico) (292073) for financial support to the first author. The authors thank the Australian National Fabrication Facility – Materials node for the provision of equipment. We thank Tania Benedetti for assistance with impedance measurements, Fletcher Thompson and Dr. Stephen Beirne for 3D printed lids for electrodes. Also, the assistance of Tony Romeo at the UOW Electron Microscopy Centre for technical expertise in SEM. We also thank Azadeh Mirabedini and Nicolas Martino for assistance with SEM, Hongrui Zhang for AFM imaging. We would like to thank Prof. Robert Kapsa, Dr. Anita Quigley and Dr. Justin Bourke for their useful advice. The authors have no financial interests to disclose.

## References

[1] Darabid H, Perez-Gonzalez AP, Robitaille R. Neuromuscular synaptogenesis: coordinating partners with multiple functions. Nature Reviews Neuroscience. 2014;15:703-18.

[2] Sanes JR, Lichtman JW. Development of the vertebrate neuromuscular junction. Annual review of neuroscience. 1999;22:389-442.

[3] Sanes JR, Lichtman JW. Induction, assembly, maturation and maintenance of a postsynaptic apparatus. Nature Reviews Neuroscience. 2001;2:791-805.

[4] Dalva MB, McClelland AC, Kayser MS. Cell adhesion molecules: signalling functions at the synapse. Nature Reviews Neuroscience. 2007;8:206-20.
[5] Lin W, Burgess RW, Dominguez B, Pfaff SL, Sanes JR, Lee K-F. Distinct roles of nerve and muscle in postsynaptic differentiation of the neuromuscular synapse. Nature. 2001;410:1057-64.
[6] Qazi TH, Mooney DJ, Pumberger M, Geißler S, Duda GN. Biomaterials based strategies for skeletal muscle tissue engineering: Existing technologies and future trends. Biomaterials. 2015;53:502-21.
[7] Wong JY, Langer R, Ingber DE. Electrically conducting polymers can noninvasively control the shape and growth of mammalian cells. Proceedings of the National Academy of Sciences. 1994;91:3201-4.
[8] Lin S, Maj M, Bezakova G, Magyar JP, Brenner HR, Ruegg MA. Muscle-wide secretion of a miniaturized form of neural agrin rescues focal neuromuscular innervation in agrin mutant mice. Proceedings of the National Academy of Sciences. 2008;105:11406-11.
[9] Willmann R, Fuhrer C. Neuromuscular synaptogenesis: clustering of acetylcholine receptors revisited. Cellular and Molecular Life Sciences CMLS. 2002;59:1296-316.
[10] Tintignac LA, Brenner H-R, Rüegg MA. Mechanisms Regulating Neuromuscular Junction Development and Function and Causes of Muscle Wasting. Physiological reviews. 2015;95:809-52.
[11] Zhang BG, Quigley AF, Bourke JL, Nowell CJ, Myers DE, Choong PF, Kapsa RM. Combination of agrin and laminin increase acetylcholine receptor clustering and enhance functional neuromuscular junction formation In vitro. Developmental neurobiology. 2015.
[12] Krakora D, Macrander C, Suzuki M. Neuromuscular Junction Protection for the Potential Treatment of Amyotrophic Lateral Sclerosis. Neurology research international. 2012;2012:379657.
[13] Hettwer S, Lin S, Kucsera S, Haubitz M, Oliveri F, Fariello RG, Ruegg MA, Vrijbloed JW. Injection of a Soluble Fragment of Neural Agrin (NT-1654) Considerably Improves the Muscle Pathology Caused by the Disassembly of the Neuromuscular Junction. PLoS ONE. 2014;9:e88739.
[14] Blankenship AG, Feller MB. Mechanisms underlying spontaneous patterned activity in developing neural circuits. Nature Reviews Neuroscience. 2010;11:18-29.
[15] Spitzer NC. Electrical activity in early neuronal development. Nature. 2006;444:707-12.
[16] McCaig CD, Rajnicek AM, Song B, Zhao M. Controlling Cell Behavior Electrically: Current Views and Future Potential2005.
[17] Meng S, Rouabhia M, Zhang Z. Electrical stimulation modulates osteoblast proliferation and bone protein production through heparin-bioactivated conductive scaffolds. Bioelectromagnetics. 2013;34:189-99.
[18] Schuhfried O, Crevenna R, Fialka-Moser V, Paternostro-Sluga T. Non-invasive neuromuscular electrical stimulation in patients with central nervous system lesions: an educational review. Journal of rehabilitation medicine. 2012;44:99-105.
[19] Gilmore KJ, Kita M, Han Y, Gelmi A, Higgins MJ, Moulton SE, Clark GM, Kapsa R, Wallace GG. Skeletal muscle cell proliferation and differentiation on polypyrrole substrates doped with extracellular matrix components. Biomaterials. 2009;30:5292-304.
[20] Stewart E, Kobayashi NR, Higgins MJ, Quigley AF, Jamali S, Moulton SE, Kapsa RM, Wallace GG, Crook JM. Electrical Stimulation Using Conductive Polymer Polypyrrole Promotes Differentiation of Human Neural Stem Cells: A Biocompatible Platform for Translational Neural Tissue Engineering. Tissue Engineering Part C: Methods. 2014.
[21] Liu X, Yue Z, Higgins MJ, Wallace GG. Conducting polymers with immobilised fibrillar collagen for enhanced neural interfacing. Biomaterials. 2011;32:7309-17.
[22] Quigley AF, Razal JM, Thompson BC, Moulton SE, Kita M, Kennedy EL, Clark GM, Wallace GG, Kapsa RMI. A Conducting-Polymer Platform with Biodegradable Fibers for Stimulation and Guidance of Axonal Growth. Advanced Materials. 2009;21:4393-7.

[23] Fukazawa T, Matsumoto M, Imura T, Khalesi E, Kajiume T, Kawahara Y, Tanimoto K, Yuge L. Electrical stimulation accelerates neuromuscular junction formation through ADAM19/neuregulin/ErbB signaling in vitro. Neuroscience letters. 2013;545:29-34.
[24] Johnson AM, Connor NP. Effects of electrical stimulation on neuromuscular junction morphology in the aging rat tongue. Muscle & nerve. 2011;43:203-11.
[25] Tomori K, Ohta Y, Nishizawa T, Tamaki H, Takekura H. Low-intensity electrical stimulation ameliorates disruption of transverse tubules and neuromuscular junctional architecture in denervated rat skeletal muscle fibers. Journal of muscle research and cell motility. 2010;31:195-205.
[26] Huang CQ, Shepherd RK, Center P, Seligman PM, Tabor B. Electrical stimulation of the auditory nerve: direct current measurement in vivo. Biomedical Engineering, IEEE Transactions on. 1999;46:461-9.
[27] Merrill DR, Bikson M, Jefferys JG. Electrical stimulation of excitable tissue: design of efficacious and safe protocols. Journal of neuroscience methods. 2005;141:171-98.
[28] Cogan SF. Neural Stimulation and Recording Electrodes. Annual Review of Biomedical Engineering. 2008;10:275-309.
[29] Balint R, Cassidy NJ, Cartmell SH. Conductive polymers: Towards a smart biomaterial for tissue engineering. Acta Biomaterialia. 2014;10:2341-53.
[30] Garner B, Hodgson AJ, Wallace GG, Underwood PA. Human endothelial cell a. Journal of Materials Science: Materials in Medicine. 1999;10:19-27.
[31] Bendrea A-D, Cianga L, Cianga I. Review paper: Progress in the Field of Conducting Polymers for Tissue Engineering Applications. Journal of biomaterials applications. 2011;26:3-84.
[32] Ravichandran R, Sundarrajan S, Venugopal JR, Mukherjee S, Ramakrishna S. Applications of conducting polymers and their issues in biomedical engineering. Journal of the Royal Society Interface. 2010;7:S559-S79.
[33] Zhang H, Molino PJ, Wallace GG, Higgins MJ. Quantifying Molecular-Level Cell Adhesion on Electroactive Conducting Polymers using Electrochemical-Single Cell Force Spectroscopy. Scientific Reports. 2015;5:13334.
[34] Stewart EM, Liu X, Clark GM, Kapsa RMI, Wallace GG. Inhibition of smooth muscle cell adhesion and proliferation on heparin-doped polypyrrole. Acta Biomaterialia. 2012;8:194-200.
[35] Quigley AF, Razal JM, Thompson BC, Moulton SE, Kita M, Kennedy EL, Clark GM, Wallace GG, Kapsa RM. A conducting-polymer platform with biodegradable fibers for stimulation and guidance of axonal growth. Advanced Materials. 2009;21:4393.
[36] Kung TA, Langhals NB, Martin DC, Johnson PJ, Cederna PS, Urbanchek MG. Regenerative peripheral nerve interface viability and signal transduction with an implanted electrode. Plastic and reconstructive surgery. 2014;133:1380-94.
[37] Green RA, Lovell NH, Wallace GG, Poole-Warren LA. Conducting polymers for neural interfaces: Challenges in developing an effective long-term implant. Biomaterials. 2008;29:3393-9.
[38] Thompson BC, Moulton SE, Ding J, Richardson R, Cameron A, O'Leary S, Wallace GG, Clark GM. Optimising the incorporation and release of a neurotrophic factor using conducting polypyrrole. Journal of controlled release : official journal of the Controlled Release Society. 2006;116:285-94.
[39] Wallace GG, Kane-Maguire LA. Manipulating and monitoring biomolecular interactions with conducting electroactive polymers. Advanced Materials. 2002;14:953-60.
[40] Thompson BC, Moulton SE, Richardson RT, Wallace GG. Effect of the dopant anion in polypyrrole on nerve growth and release of a neurotrophic protein. Biomaterials. 2011;32:3822-31.

[41] Thompson BC, Richardson RT, Moulton SE, Evans AJ, O'Leary S, Clark GM, Wallace GG. Conducting polymers, dual neurotrophins and pulsed electrical stimulation — Dramatic effects on neurite outgrowth. Journal of Controlled Release. 2010;141:161-7.
[42] Richardson RT, Thompson B, Moulton S, Newbold C, Lum MG, Cameron A, Wallace G, Kapsa R, Clark G, O'Leary S. The effect of polypyrrole with incorporated neurotrophin-3 on the promotion of neurite outgrowth from auditory neurons. Biomaterials. 2007;28:513-23.
[43] Bolto B, McNeill R, Weiss D. Electronic Conduction in Polymers. III. Electronic Properties of Polypyrrole. Australian Journal of Chemistry. 1963;16:1090-103.
[44] Gelmi A, Higgins MJ, Wallace GG. Physical surface and electromechanical properties of doped polypyrrole biomaterials. Biomaterials. 2010;31:1974-83.
[45] Higgins MJ, Molino PJ, Yue Z, Wallace GG. Organic conducting polymer–protein interactions. Chemistry of Materials. 2012;24:828-39.
[46] Sherrell PC, Thompson BC, Wassei JK, Gelmi AA, Higgins MJ, Kaner RB, Wallace GG. Maintaining cytocompatibility of biopolymers through a graphene layer for electrical stimulation of nerve cells. Advanced functional materials. 2014;24:769-76.
[47] Matusica D, Fenech MP, Rogers M-L, Rush RA. Characterization and use of the NSC-34 cell line for study of neurotrophin receptor trafficking. Journal of Neuroscience Research. 2008;86:553-65.
[48] Cashman NR, Durham HD, Blusztajn JK, Oda K, Tabira T, Shaw IT, Dahrouge S, Antel JP. Neuroblastoma × spinal cord (NSC) hybrid cell lines resemble developing motor neurons. Developmental Dynamics. 1992;194:209-21.
[49] Vaarmann A, Gandhi S, Gourine AV, Abramov AY. Novel pathway for an old neurotransmitter: Dopamine-induced neuronal calcium signalling via receptor-independent mechanisms. Cell calcium. 2010;48:176-82.
[50] Gandhi S, Vaarmann A, Yao Z, Duchen MR, Wood NW, Abramov AY. Dopamine Induced Neurodegeneration in a PINK1 Model of Parkinson's Disease. PLoS ONE. 2012;7:e37564.
[51] Bourke JL, Coleman HA, Pham V, Forsythe JS, Parkington HC. Neuronal Electrophysiological Function and Control of Neurite Outgrowth on Electrospun Polymer Nanofibers Are Cell Type Dependent. Tissue Engineering Part A. 2013;20:1089-95.
[52] Maier O, Böhm J, Dahm M, Brück S, Beyer C, Johann S. Differentiated NSC-34 motoneuron-like cells as experimental model for cholinergic neurodegeneration. Neurochemistry international. 2013;62:1029-38.
[53] Tse N, Morsch M, Ghazanfari N, Cole L, Visvanathan A, Leamey C, Phillips WD. The Neuromuscular Junction: Measuring Synapse Size, Fragmentation and Changes in Synaptic Protein Density Using Confocal Fluorescence Microscopy. 2014:e52220.
[54] Anselme K. Osteoblast adhesion on biomaterials. Biomaterials. 2000;21:667-81.
[55] Sanes J, Lichtman J. Development of the vertebrate neuromuscular junction. Annual Review of Neuroscience. 1999;22:389-442.
[56] Reist N, Werle M, McMahan U. Agrin released by motor neurons induces the aggregation of acetylcholine receptors at neuromuscular junctions. Neuron. 1992;8:865-8.
[57] Xie Z, Poo M. Initial events in the formation of neuromuscular synapse: rapid induction of acetylcholine release from embryonic neuron. Proceedings of the National Academy of Sciences of the United States of America. 1986;83:7069.
[58] Morimoto Y, Kato-Negishi M, Onoe H, Takeuchi S. Three-dimensional neuron–muscle constructs with neuromuscular junctions. Biomaterials. 2013;34:9413-9.
[59] Guo X, Gonzalez M, Stancescu M, Vandenburgh HH, Hickman JJ. Neuromuscular junction formation between human stem cell-derived motoneurons and human skeletal muscle in a defined system. Biomaterials. 2011;32:9602-11.
[60] Xiong GM, Do AT, Wang JK, Yeoh CL, Yeo KS, Choong C. Development of a miniaturized stimulation device for electrical stimulation of cells. Journal of Biological Engineering. 2015;9:14.

[61] Peckham PH, Knutson JS. Functional Electrical Stimulation for Neuromuscular Applications. Annual Review of Biomedical Engineering. 2005;7:327-60.
[62] Merrill DR, Bikson M, Jefferys JGR. Electrical stimulation of excitable tissue: design of efficacious and safe protocols. Journal of Neuroscience Methods. 2005;141:171-98.
[63] Cossins J, Burke G, Maxwell S, Spearman H, Man S, Kuks J, Vincent A, Palace J, Fuhrer C, Beeson D. Diverse molecular mechanisms involved in AChR deficiency due to rapsyn mutations. Brain : a journal of neurology. 2006;129:2773-83.
[64] Lu B, Czernik A, Popov S, Wang T, Poo M-M, Greengard P. Expression of synapsin I correlates with maturation of the neuromuscular synapse. Neuroscience. 1996;74:1087-97.
[65] Fahim MA, Holley JA, Robbins N. Topographic comparison of neuromuscular junctions in mouse slow and fast twitch muscles. Neuroscience. 1984;13:227-35.
[66] Desaki J, Uehara Y. The overall morphology of neuromuscular junctions as revealed by scanning electron microscopy. Journal of neurocytology. 1981;10:101-10.
[67] Zhang HL, Peng HB. Mechanism of Acetylcholine Receptor Cluster Formation Induced by DC Electric Field. PLoS ONE. 2011;6:e26805.
[68] Kramer JF. Effect of electrical stimulation current frequencies on isometric knee extension torque. Physical therapy. 1987;67:31-8.
[69] Grimby L, Hannerz J. Firing rate and recruitment order of toe extensor motor units in different modes of voluntary conraction. The Journal of Physiology. 1977;264:865-79.
[70] Stauffer WR, Cui XT. Polypyrrole doped with 2 peptide sequences from laminin. Biomaterials. 2006;27:2405-13.
[71] Zhang L, Stauffer WR, Jane EP, Sammak PJ, Cui XT. Enhanced differentiation of embryonic and neural stem cells to neuronal fates on laminin peptides doped polypyrrole. Macromolecular bioscience. 2010;10:1456-64.

**Figure 1:** Materials characterization. **A, B)** Atomic force microscopy (AFM) topographic images of the gold coated mylar films (RMS value of 1.17 nm) at 10 and 1 $\mu m^2$ area respectively. **C)** Scanning electrode microscope (SEM) image of the gold coated film, scale bar 10 µm. **D, E)** Atomic force microscope (AFM) topographic images of the PPy/DBS gold coated mylar films (RMS value of 4.26 nm) of 10 and 1 µm square areas respectively with sampling size of 512 x 512 pixels. **F)** Scanning electrode microscope (SEM) image of the PPy/DBS gold coated mylar film, scale bar 10 µm. **G)** Impedance spectra for gold coated mylar and PPy/DBS gold coated mylar films recorded in PBS (pH = 7.2) at +50.0 mV (vs Ag|AgCl) recorded between 0.01 Hz and 100 kHz. **H)** An example of the biphasic current waveform (green), overlaid with the output voltage obtained from the two-electrode system using PPy/DBS gold coated mylar (red) and gold coated mylar (blue) without cells.

**Figure 2**: Development of co-cultures of nerve and muscle. **A)** Individual fluorescence channels of cell**s** stained for DAPI (nuclear stain, blue), β-III tubulin (neural stain, green), desmin (muscle stain, red), and alpha-bungarotoxin (Ach receptor stain, purple) Scale bar indicates 40 µm. **B)** Overlay image of a co-culture of primary myoblast (muscle) and NSC-34 (motor neuron) cells. Cell**s** stained for DAPI (nuclear stain, blue), β-III tubulin (neural stain, green), desmin (muscle stain, red), and alpha-bungarotoxin (Ach receptor stain, purple). Scale bar indicates 40 µm. **C)** Scanning electron microscope image showing the morphologies of muscle and nerve cells in a co-culture environment. Arrows indicate differentiated myotubes, stars indicate NSC-34 cells. Scale bar indicates 10 µm.

**Figure 3**: $Ca^{2+}$ imaging responses of the NSC-34 and primary myoblast mono-cultures and co-cultures, to stimulation using glutamic acid. **A)** Graph representing calcium transient responses caused by the glutamic acid, this is indicated by three regions of interest (ROI) on the fluorescent channel alongside bright field image with two NSC-34 and one control trace (no cells). Red arrows indicate addition of glutamic acid **B)** Graph representing calcium

transient responses of active (twitching) muscle to either glutamic acid (no change) or high potassium. This is indicated by two ROIs containing active twitching muscle cells (blue and green traces) and one inactive muscle (no twitching, orange trace), as well as a control trace (no active cells, red trace). The fluorescence (Fluo-4) vs time traces correspond to cells indicated on the fluorescence and bright field images. Red arrows indicate addition of glutamic acid and the blue arrow indicates addition of potassium. **C)** The graph represents calcium transient responses of active muscle (twitching) in co-cultures to glutamic acid. This is indicated by three ROIs containing two active muscle cells (twitching) and one control trace (no active cells) on the fluorescent channel alongside bright field image. Arrows indicate the addition of glutamic acid. Scale bars represent 25 µm.

**Figure 4**: Electrical stimulation scheme for stimulating cultures of nerve, muscle and co-cultures on electroactive PPy/DBS gold coated mylar. **A)** Photographs of the custom cell culture and stimulation module showing the platinum mesh (arrows) counter electrodes and cell culture chambers on gold–coated mylar (left) and PPy/DBS gold coated mylar (right). **B)** An example of the biphasic current waveform (green), overlaid with the output voltage obtained in the two-electrode system stimulating with (blue) and without (red) cells using PPy/DBS gold coated mylar. The stimulus waveform had an applied current of 1 $mA/cm^2$, with a biphasic pulse of 100 µs pulses with 20 µs interphase open circuit and 3.78 ms short circuit phase at a frequency of 250 Hz. **C)** Schematic of cell culture and stimulation setup illustrating the working and counter electrodes. **D)** COMSOL modelling of the current density on the working electrode **(**fraction deviation from average current density**,** $mA/cm^2$) illustrating the expected distribution between the two electrode surfaces. Scale bar represents 500 µm.

**Figure 5**: Effect of electrical stimulation parameters on the number of AChR clusters. Effect of ES on number of AChR clusters in co-cultures using different **(A)** frequencies, **(B)** current amplitudes and **(C)** durations of stimulation. Each parameter was tested in three independent experiments (n=3) with 60 total images, error bars represent the standard deviation. ‘‘*’’ indicates statistical significance, $p \leq 0.01$. **D)** Close up of a region containing a muscle fiber with AChRs stained using alpha bungarotoxin. Scale bar represents 20 µm.

**Figure 6**: Effect of electrical stimulation using different electrode materials. **A)** Effect of ES on the number of AChR clusters of co-cultures using PPy/DBS gold coated mylar, compared to the gold coated mylar substrate. **B)** Effect of ES on the number of AChR clusters of muscle monocultures on PPy/DBS gold coated mylar, compared to the gold coated mylar substrate. For A) and B), each parameter was tested in three independent experiments (n=3) with 60 and 40 total images respectively, error bars represent the standard deviation. ‘‘*’’ indicates statistical significance, $p \leq 0.0001$. **C)** Effect of electrical stimulation on the expression of Rapsyn and Synapsin proteins, relative to the loading control β-actin, in co-cultures and also in nerve and muscle monocultures. Error bars represent the standard error of the mean. **D)** Western blot data supporting the increase in protein expression of Rapsyn and Synapsin on PPy/DBS gold coated mylar electrodes.

**Figure 7:** Clustering of ACh receptors in muscle mono-cultures and co-cultures, indicated by arrows. **A**) SEM image of AChR clusters in co-cultures, scale bars represent 1µm. **B)** SEM image of AChR clusters in muscle; scale bars represent 1µm. **C**) AChR clusters without electrical stimulation in co-culture. **D**) AChR clusters after electrical stimulation in co-culture. **E)** AChR clusters in muscle monocultures without electrical stimulation. **F**) AChR clusters in muscle monocultures after electrical stimulation. Scale bars represent 20 µm. **G)** Graphical representation of the effect of ES on AChR cluster sizes. Co-culture data was obtained from three independent experiments (n=3) with 36 total images, muscle cell data was obtained from

three independent experiments (n=3) with 24 total images. Error bars represent the standard error of the mean. * indicates statistical significance, $p \leq 0.05$.

***Graphical Abstract**

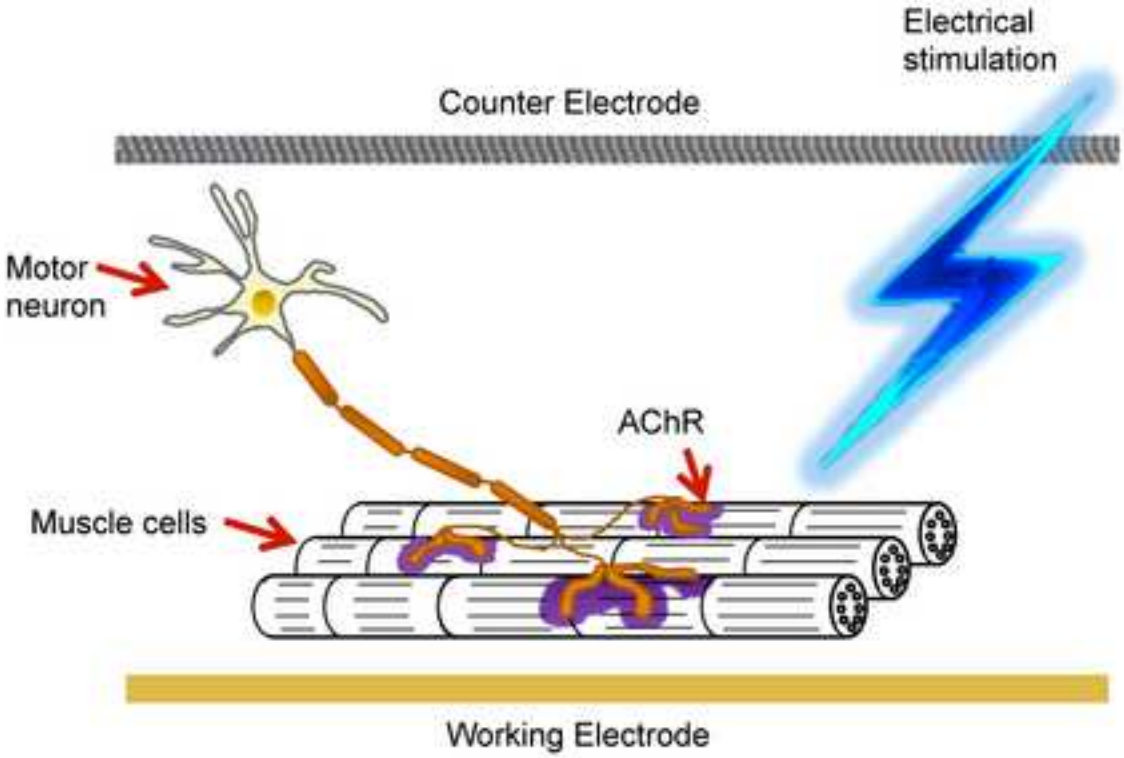

Figure(s)

Click here to download high resolution image

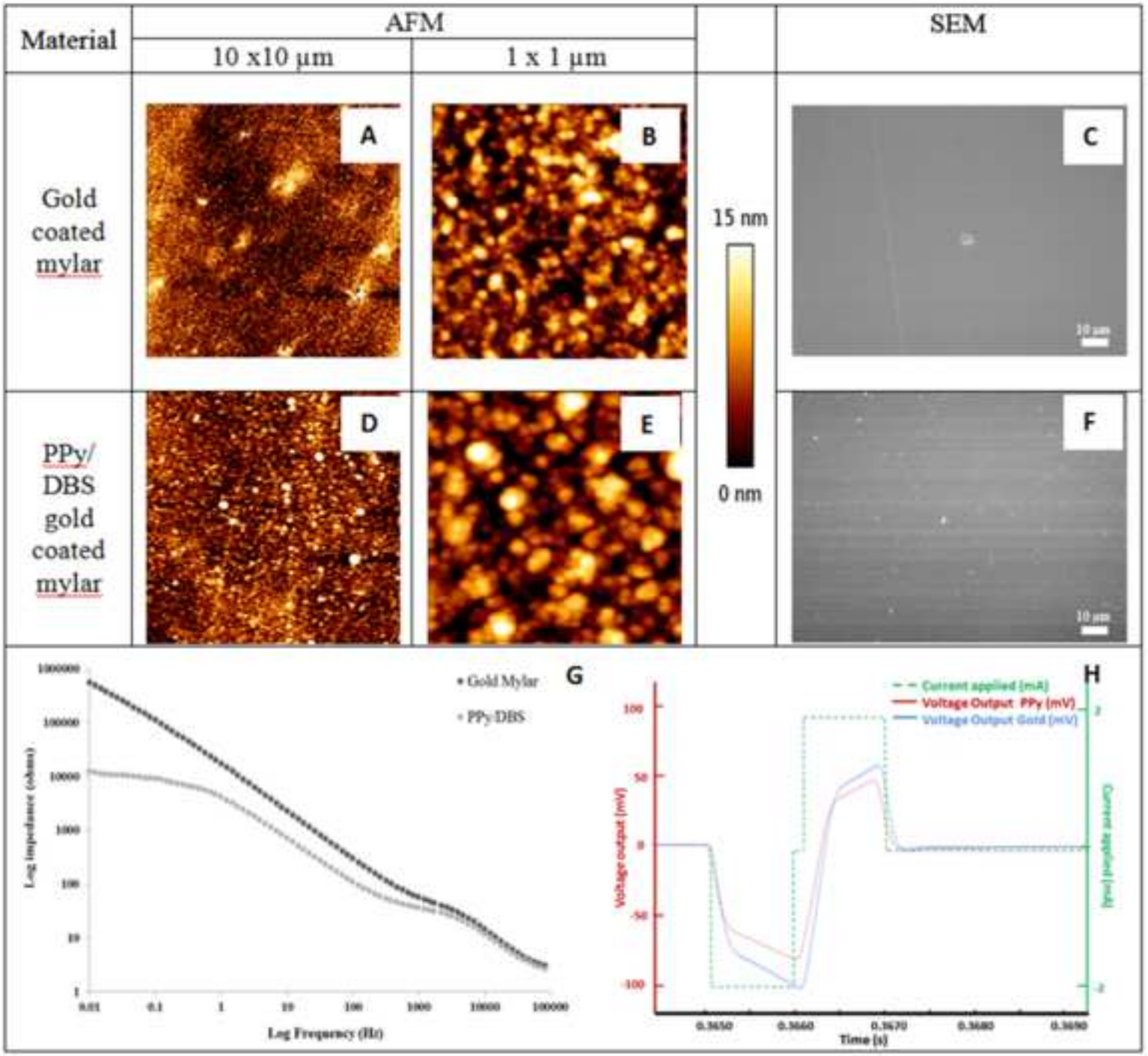

**Figure(s)**

**Click here to download high resolution image**

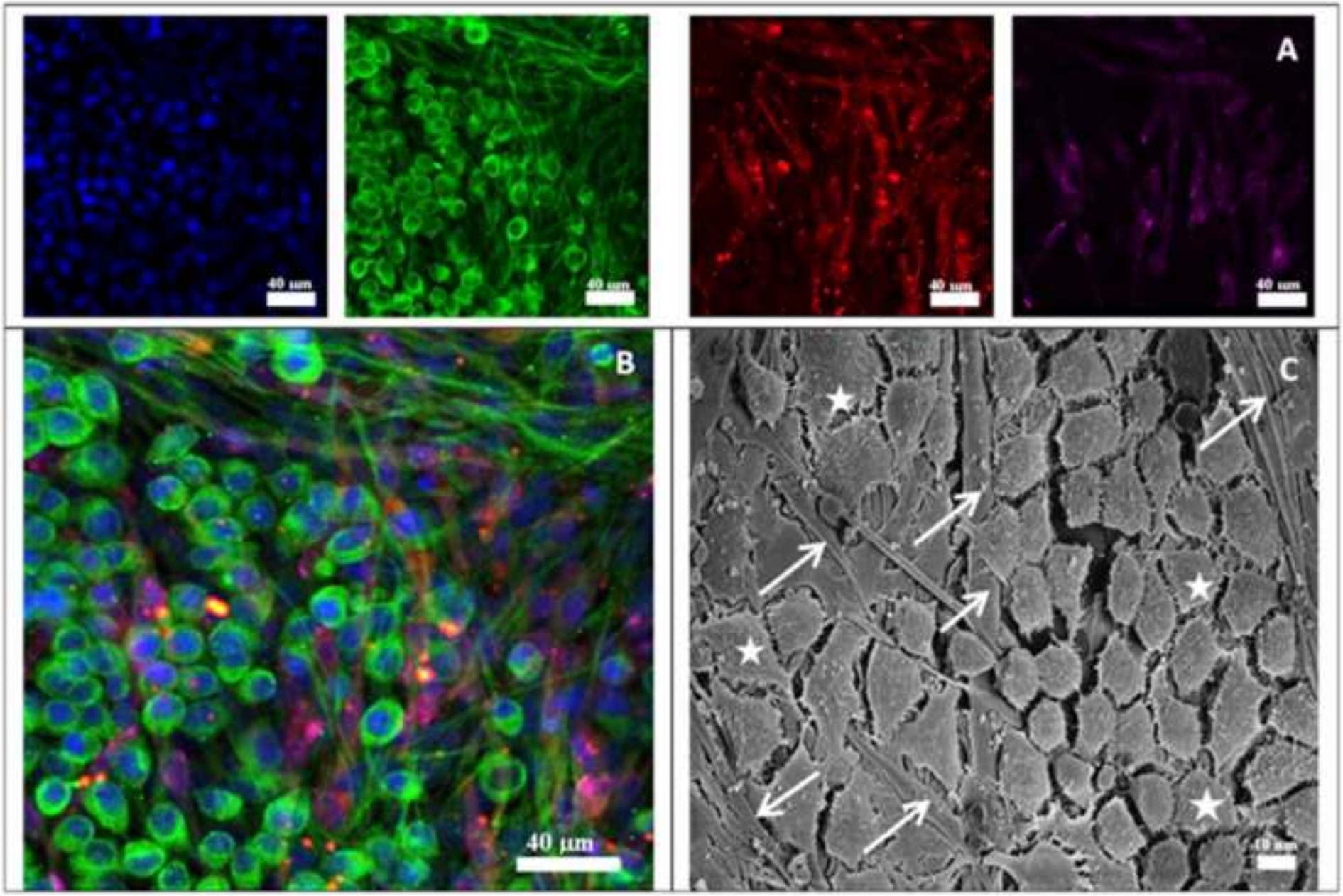

Figure(s)

Click here to download high resolution image

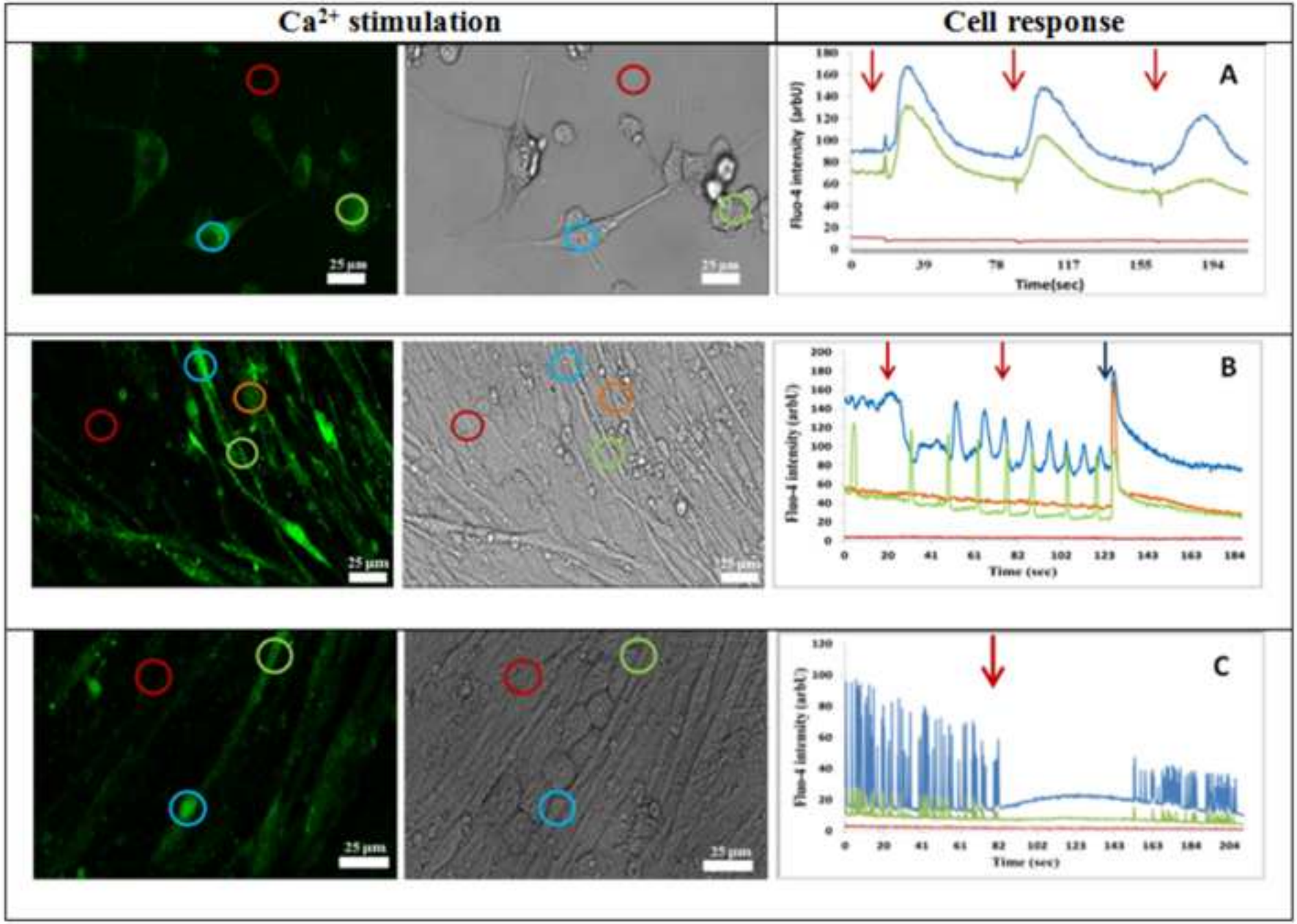

Figure(s)

Click here to download high resolution image

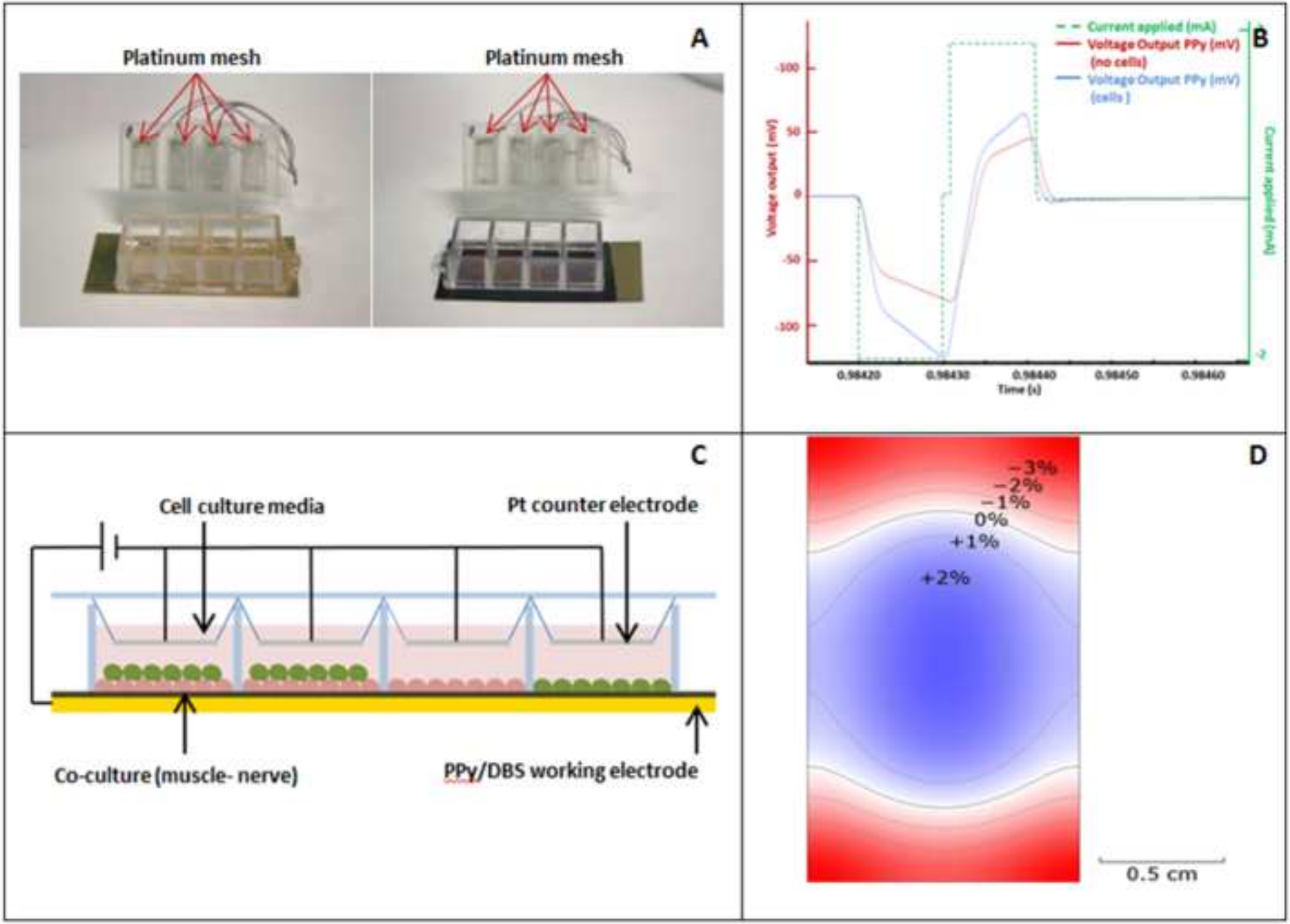

Figure(s)

Click here to download high resolution image

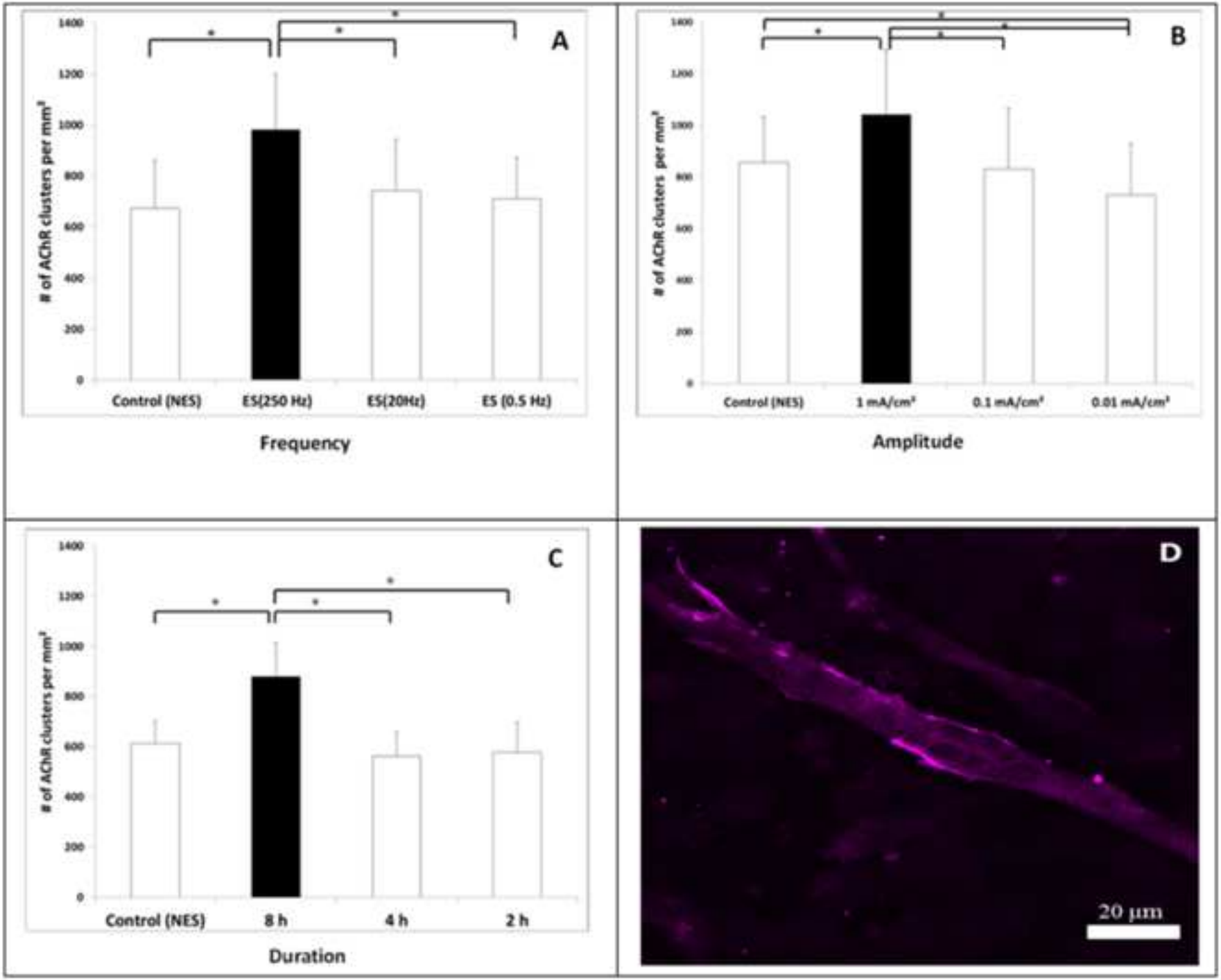

Figure(s)

Click here to download high resolution image

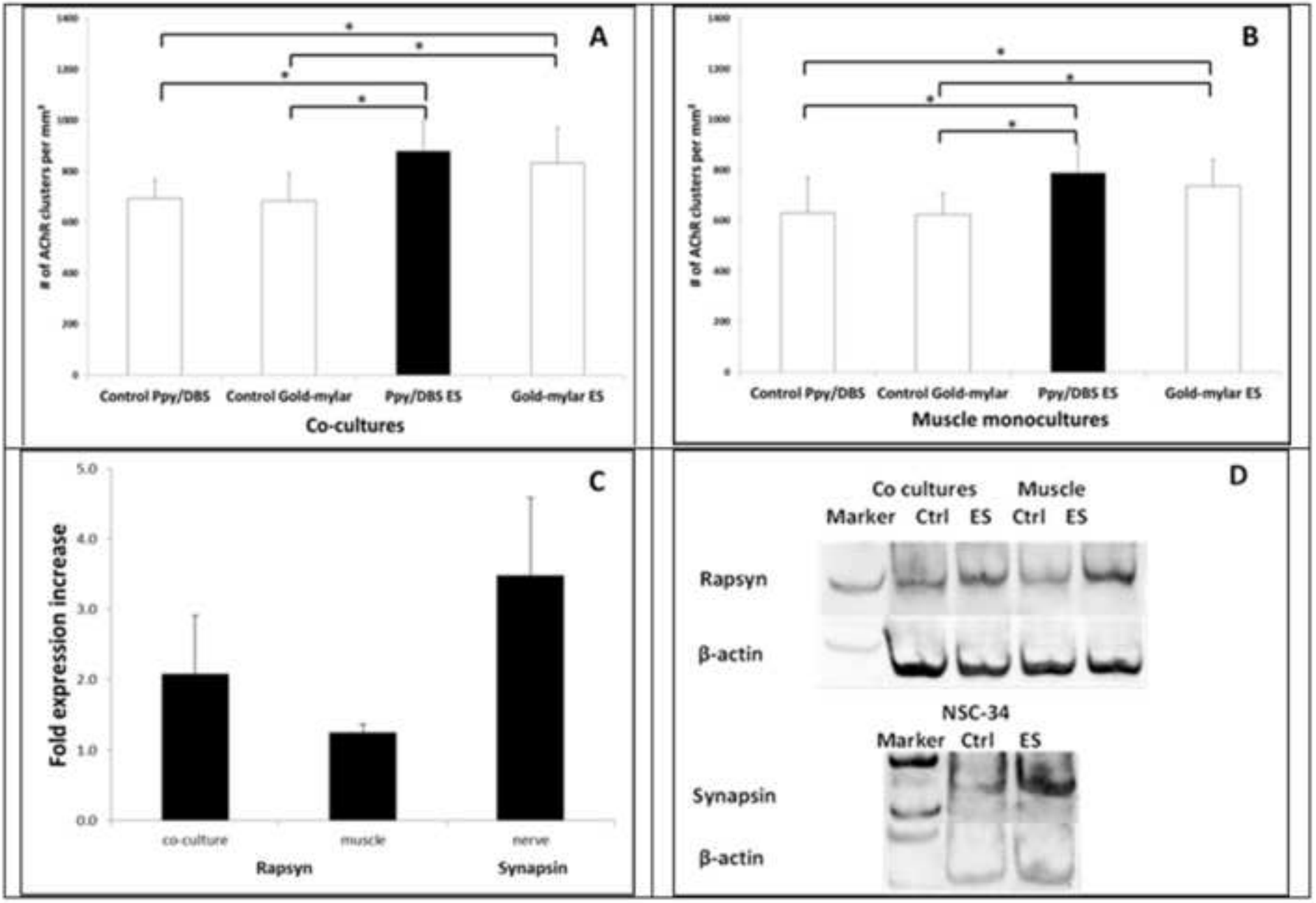

Figure(s)

Click here to download high resolution image

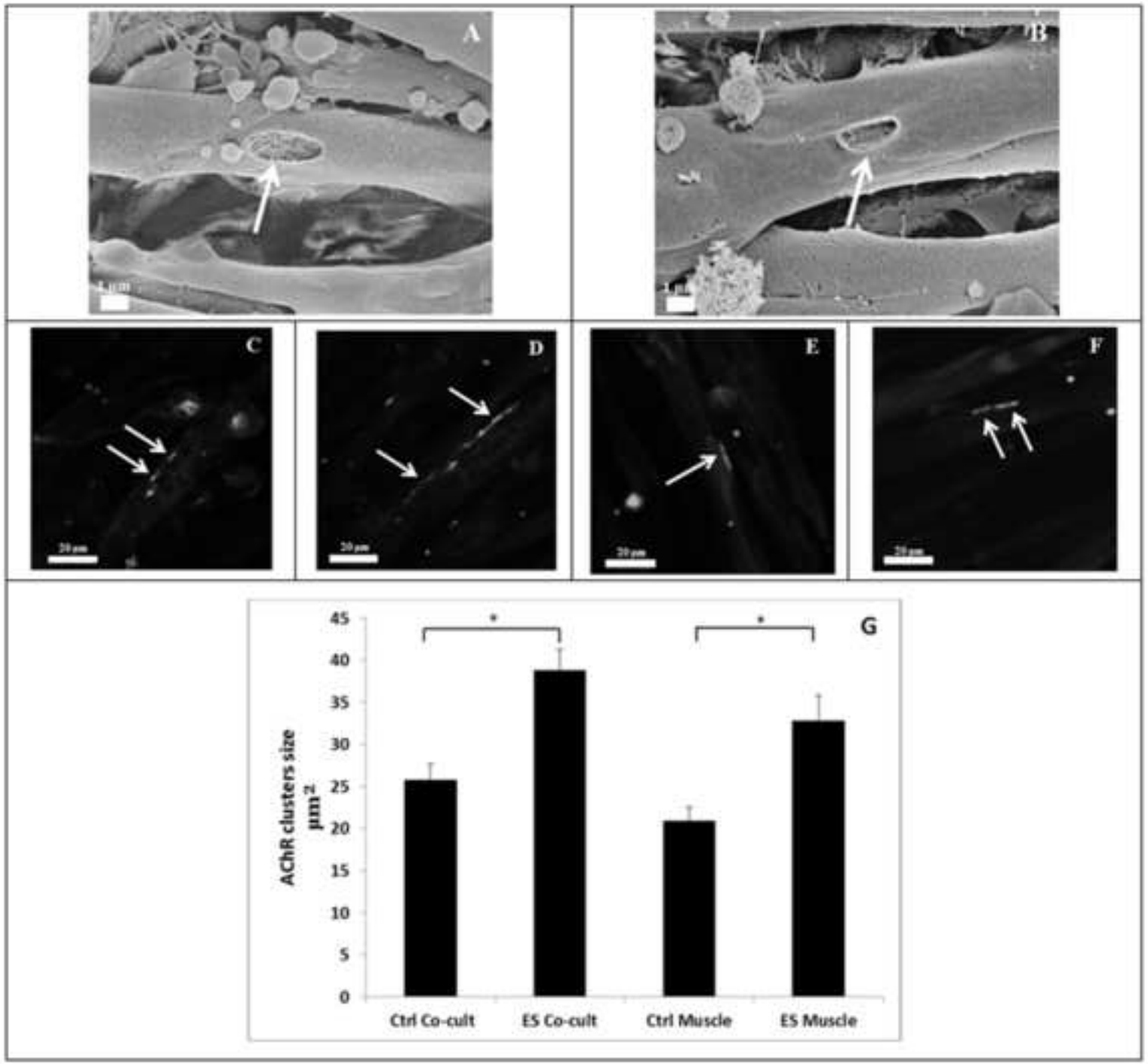

**Supplementary Material**

**Click here to download Supplementary Material: Supplementary material.docx**

**Video Still**

**Click here to download high resolution image**

**Video Still**

**Click here to download high resolution image**

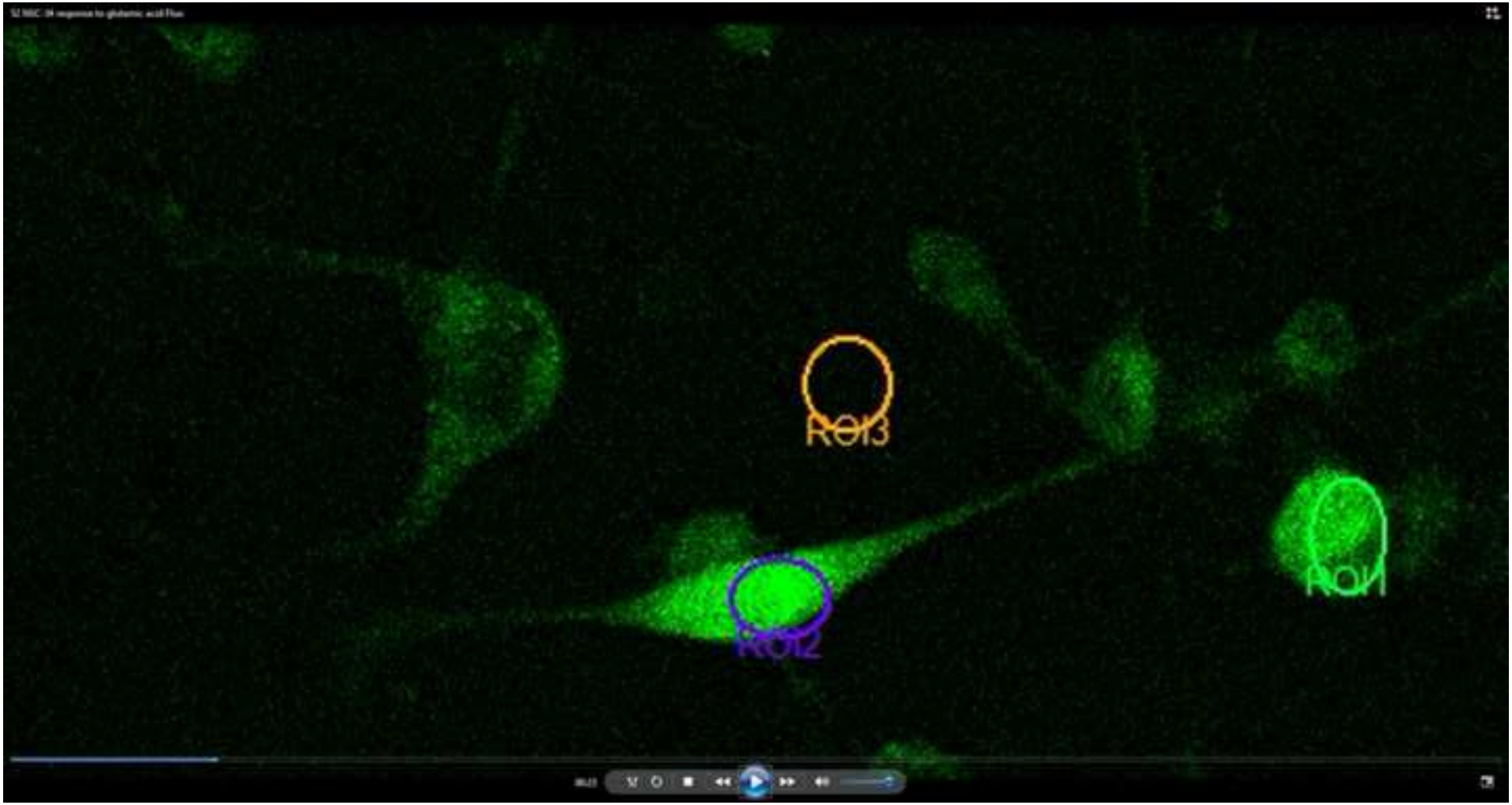

**Video Still**

**Click here to download high resolution image**

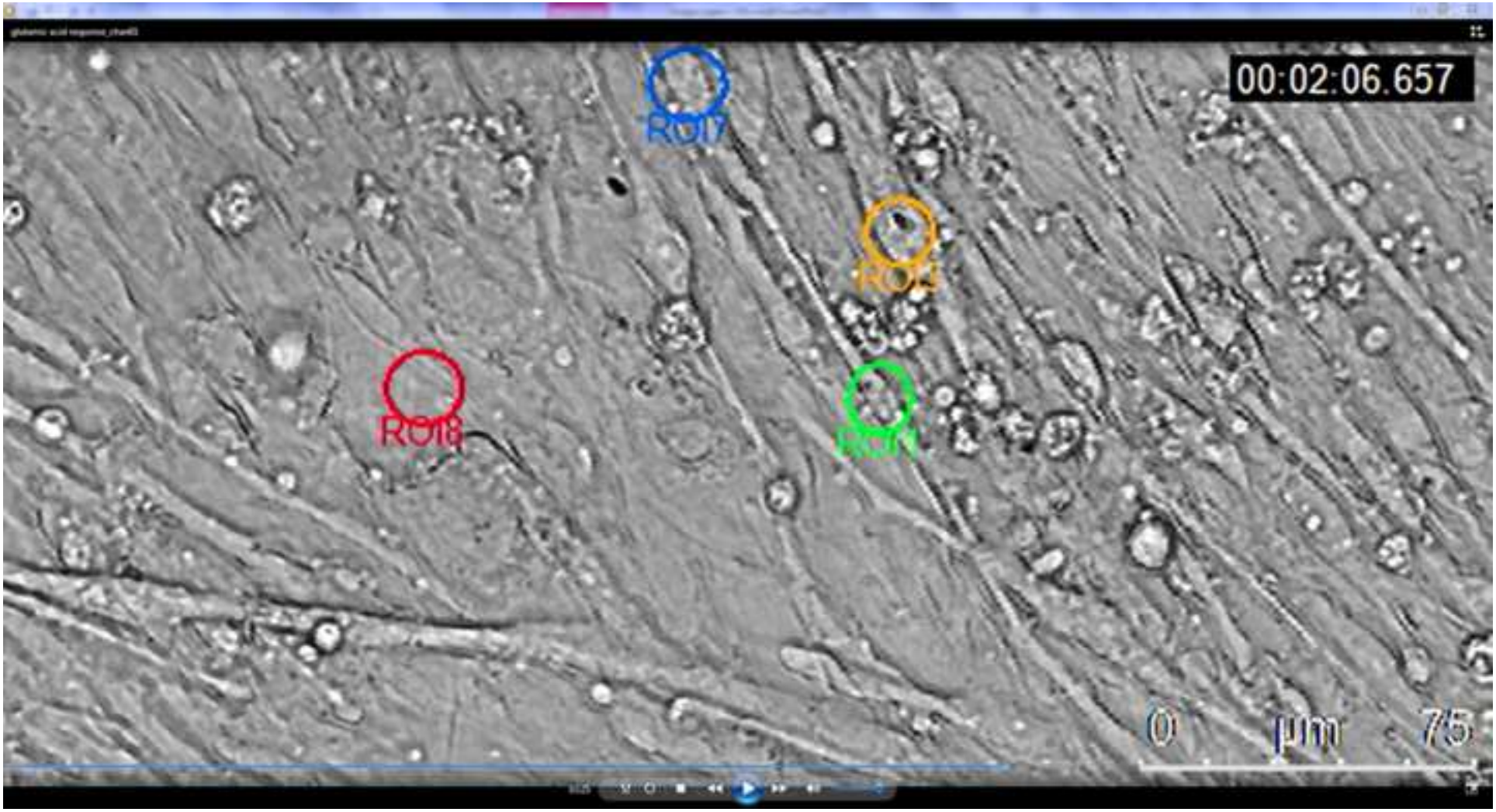

**Video Still**

**Click here to download high resolution image**

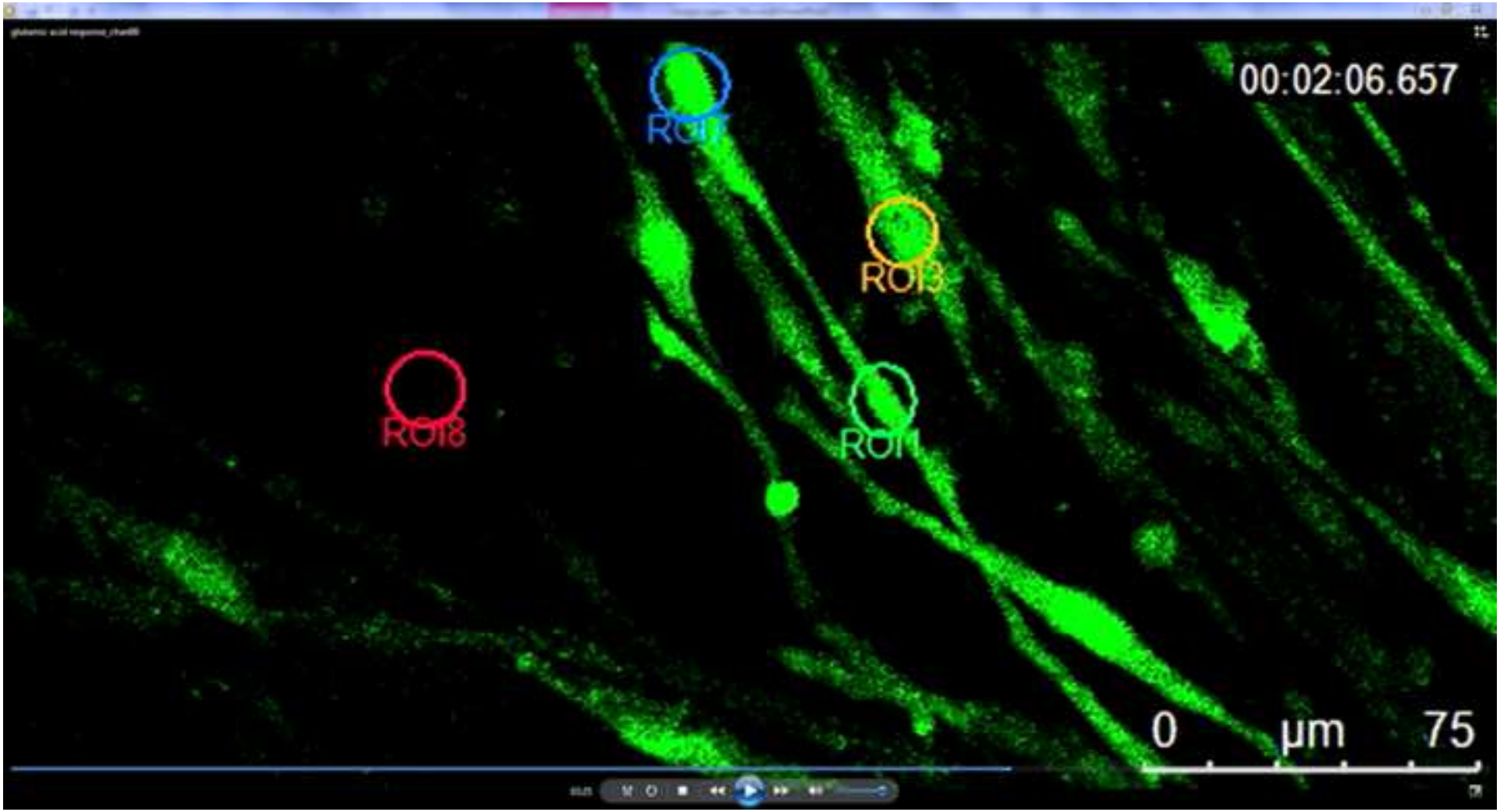

**Video Still**

**Click here to download high resolution image**

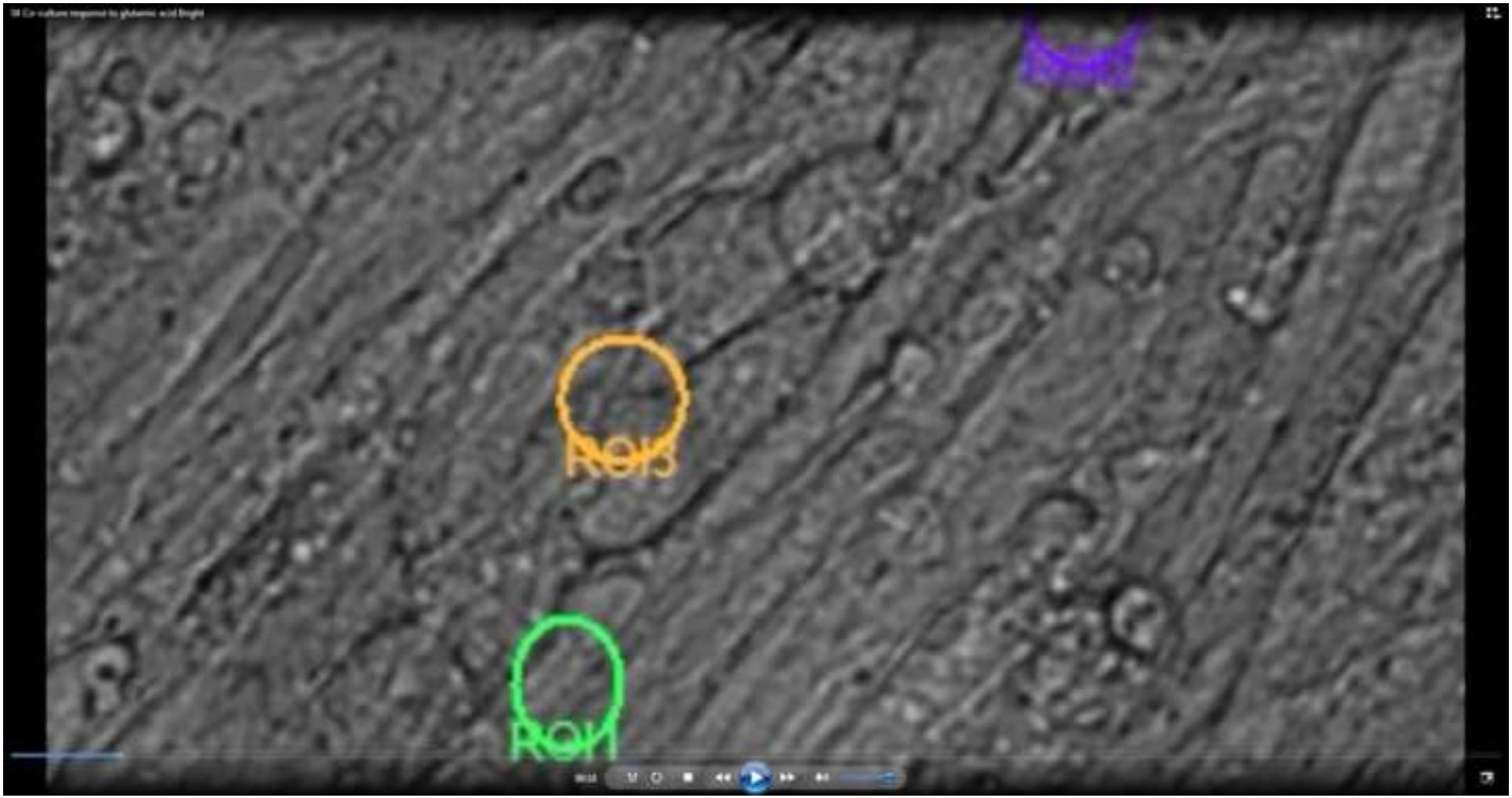

**Video Still**

**Click here to download high resolution image**